# Decoding water-rock interaction and volatile input at La Soufriere volcano (Guadeloupe) using time-series major and trace element analyses in gas condensates

Manuel Inostroza, Séverine Moune, Roberto Moretti, Magali Bonifacie, Vincent Robert, Arnaud Burtin, Elodie Chilin-Eusebe

Version of Record: https://www.sciencedirect.com/science/article/pii/S0377027322000488
Manuscript_466e3352205a5516356a4147515ad930

# Decoding water-rock interaction and volatile input at La Soufriere volcano (Guadeloupe) using time-series major and trace element analyses in gas condensates

Manuel Inostroza[1,2*], Séverine Moune[1,2,3], Roberto Moretti[1,2], Magali Bonifacie[1,2], Vincent Robert[1,2], Arnaud Burtin[1], Elodie Chilin-Eusebe[1,2]

[1]Université de Paris, Institut de Physique du Globe de Paris, CNRS, F75005, Paris, France

[2]Observatoire Volcanologique et Sismologique de Guadeloupe, Institut de Physique du Globe de Paris, F97113, Gourbeyre, France.

[3]CNRS, IRD, OPCG Laboratoire Magmas et Volcans, Université Clermont Auvergne, F63000, Clermont-Ferrand, France

*Corresponding Author: inostroza@ipgp.fr; manuelinostrozap@gmail.com

## Abstract

The geochemical behavior of major and trace elements in fumarolic gas condensate samples collected between April 2017 and January 2021 was investigated at La Soufriere hydrothermal volcano. Samples collected from Cratère Sud and Napoleon Nord fumaroles (temperature varying from 93.9 to 108.4 °C) offer a unique opportunity to reveal the physicochemical processes that affect the deeper magmatic and shallow hydrothermal systems feeding fumaroles. Gas condensate samples exhibit abundant solid particles that suggest strong water-rock interaction and erosive processes in fumarolic conduits at La Soufriere. These particles were incorporated during sampling, except for rare Si-rich spherules that appeared to have precipitated during storage time. Gas condensate samples displayed abundant concentrations of S, halogens (Cl, Br, I), metals/metalloids (B, Ni, Cu, Zn, As, Mo, Ag, Cd, Sb, Pb, and Bi), as well as enhanced concentrations of rock-related lithophile and siderophile elements. The relative abundance of major and trace elements in gas condensates suggests the permanent contribution of volatile-rich magmatic fluids and strong water-rock interaction processes.

Based on elemental correlations and the physical properties of chemical elements, it is postulated that most of them are discharged in the aerosol phase, except for the halogens and S, which can be found in the gaseous phase in low-temperature fumarolic emissions. Metals and metalloids (Sb, Bi, Zn, Mo, Ni, Ag, Cd, As, and Pb) enriched in gas condensates were transported within tiny aqueous droplets, while rock-related elements (including REEs) were transported in the aerosol phase. Trace element enrichments in La Soufriere's condensates are comparable with those found in worldwide magmatic-hydrothermal systems such as Kawaj Ijen (Indonesia), Lastarria (Chile), and White Island (New Zealand) volcanoes. The size of the hydrothermal system and the degree of water-rock interaction are thought to be important parameters in controlling the abundance of major and trace elements in low-temperature fumarolic discharge.

## Highlights

The chemical composition of gas condensates is investigated

Major and trace elements are mostly released in the aerosol phase

Sulfur and halogens can be emitted in the gaseous phase

Volatile-rich magmatic input and water-rock interaction processes are assessed

Significant amounts of Sb, Bi, and Zn are discharged from La Soufriere fumaroles

## Keywords

Trace elements; hydrothermal systems; La Soufriere volcano; water-rock interaction; aerosols

## 1. Introduction

Volcanic emissions represent the most important natural sources of gases and particles into the atmosphere during quiescent degassing and eruptive periods. Indeed, volcanic emissions contribute to the natural atmospheric cycles of many gas species and trace elements (e.g., Aiuppa et al. 2003; Calabrese et al. 2011). Besides the major ($H_2O$, $CO_2$, $SO_2$, $H_2S$, HCl, HF) and minor ($N_2$, rare gases, CO, $CH_4$, $H_2$) components, it has been well known since the early work by Zoller et al. (1974) that volcanic gases and aerosols are considerably enriched in many trace elements including alkalis, alkali-earth elements, transition elements, and heavy metals

relative to host rocks. Such trace element enrichments are ubiquitously observed in gaseous emanations from volcanoes worldwide, provided when the magma temperature is high enough to ensure their volatilization (e.g., Le Guern 1988; Symonds et al. 1994; Delmelle and Stix 2000, and references therein). Trace elements are directly volatilized from a magmatic source or removed from wall rocks due to erosive processes, and are then emitted in the gas and aerosol phases. A fraction of the trace elements is trapped in the fumarolic mouth at the surface to form sublimates and incrustations due to the sharp temperature decrease and reaction with surrounding rocks. Work on volcanogenic trace elements has increased markedly during the last two decades, focusing on the understanding of deep ore-forming fluids (e.g., Scher et al. 2013; Keith et al. 2018), speciation and transport (e.g., Aiuppa et al. 2003; Moune et al. 2010), mineral forming processes (e.g., Yudovskaya et al. 2008; Sainlot et al. 2020), geochemical cycling of volcanogenic elements (e.g., Pyle and Mather 2003; Kagoshima et al. 2015), and atmospheric, environmental, and health issues (e.g., Varrica et al. 2014; Edmonds et al. 2015; Ilyinskaya et al. 2017; Stefánsson et al. 2017).

Volcanic trace elements are commonly studied via filter samples, sublimates, and incrustations (e.g., Allard et al. 2000; Gauthier et al. 2016; Zelenski et al. 2013; Sainlot et al. 2020; Inostroza et al. 2020). However, the use of condensation techniques has been limited and occasionally subject to inaccuracy problems due to the recurrent presence of colloidal sulfur which can remove chalcophile elements from the solution (e.g., Fischer et al. 1998; Shevko et al. 2018). Nevertheless, this technique has been proven to be appropriate to estimate trace element concentrations (e.g., Taran et al. 1995; Fischer et al. 1998; Zelenski et al. 2014). Condensation techniques have been restricted to a few volcanic sites with frequent high-temperature fumarolic emissions, mainly focused on trace element volatility and thermochemical modeling of fluid-rock interactions (e.g., Symonds et al. 1990, 1996; Taran et al. 1995; Africano and Bernard 2000; Zelenski et al. 2013, 2014; Kalacheva et al. 2016). However, low-temperature hydrothermal-dominated systems remain poorly studied, likely due to secondary processes (i.e., precipitation and dissolution of mineral phases, the input of meteoric water, and "contamination" by leaching of host-rock components) occurring within the hydrothermal system (Stoiber and rose 1970; Symonds et al. 1990; Taran et al. 1995) that could modify or hide the magmatic signature.

The concentration of trace elements in fumarolic emissions mainly depends on outlet gas temperature, chemical composition of fumarolic gases, and magma composition (Symonds et

al. 1990, 1992, 1996; Africano and Bernard 2000; Moune et al. 2010; Edmonds et al. 2018). It has been postulated that high-temperature and Cl-rich fumarolic emissions present higher concentrations of trace elements compared with low-temperature hydrothermal-dominated fumaroles due to the higher vapor pressure of metal-bearing species as temperature increases and the fact that Cl is a common ligand (Gauthier et al. 2016; Scholtysik and Canil 2020; Mandon et al. 2020). However, despite several works on medium- to high-temperature fumarolic emissions, little attention has been paid to major and trace element concentrations in low-temperature (~100°C) fumaroles. Consequently, deep (magmatic) and shallow (hydrothermal) physicochemical processes controlling the abundance of these elements and their transport modes remain poorly understood for steam-rich fumarolic gases.

Here we present results for gas condensate samples collected monthly between April 2017 and January 2021 at La Soufriere de Guadeloupe (hereafter La Soufriere) in the Lesser Antilles. La Soufriere is a hydrothermal-dominated volcanic system that suffered recent phreatic explosions (e.g., Le Guern et al. 1980; Komorowski 2005) and is one of the most active and dangerous volcanoes in the Lesser Antilles Arc. It currently presents permanent fumarolic activity associated with low-temperature (from 94 up to 111 °C in the investigated period) and steam-rich (commonly >95 mol%) emissions. Thus, this volcano provides a suitable environment to improve our understanding of the different parameters involved in the behavior of trace elements in volcanic condensates. In this study, major and trace element data obtained from gas condensate samples at La Soufrière's fumaroles are used to i) characterize, physically and chemically, the fumarolic degassing in terms of volatile versus non-volatile contribution of trace elements in condensates given their relative volatility, and ii) constrain the factors that control the abundance of major and trace elements. Our findings have particular relevance for understanding the transport of chemical elements in low-temperature hydrothermal emissions.

## 2. Geological Background

La Soufriere is an andesitic composite volcano situated in the Lesser Antilles volcanic arc (16.0446°N, 61.6642°W, 1467 m.a.s.l.; Fig. 1a), which has been formed by the subduction of the Atlantic plate below the Caribbean one. La Soufriere has been built up over the last 11500 years BP (Komorowski 2005; Boudon et al. 2008), experiencing recurrent magmatic and non-magmatic eruptions. The last magmatic eruption occurred in 1530 AD and was triggered by an andesitic magma intrusion at a shallow level, which caused a partial collapse of the SW flank, and was followed by a sub-plinian eruptive phase culminating in the growth of the current

summit dome (Boudon et al. 2008; Komorowski et al. 2008). Subsequent volcano-stratigraphic studies have revealed a more recent magmatic eruption in 1657 AD (Metcalfe et al. 2021), while recurrent phreatic explosions were recorded in 1797-98, 1836-37, 1956, and 1976-77 (e.g., Legendre 2012; Hincks et al. 2014). From 1992, after a decade of post-eruptive quiescence, La Soufrière entered a new phase of fumarolic and seismic unrest, whose evolution has been described in detail in previous works (Komorowski 2005; Allard et al. 2014; Villemant et al. 2014; Rosas-Carbajal et al. 2016; Tamburello et al. 2019; Moretti et al. 2020a; Jessop et al. 2021; Metcalfe et al. 2021).

Hydrothermal activity at La Soufriere is caused by the input of heat and gases coming from an andesitic magma chamber (located at a depth of 6-7 km below the summit) into shallow aquifers mainly fed by meteoric waters (Boudon et al. 2008; Villemant et al. 2014; Pichavant et al. 2018). Deep magmatic gases likely rise through fractures and fissures until they cool, condense, and interact with water hosted in reservoir rocks several hundreds of meters below the summit (Rosas-Carbajal et al. 2016). Previous studies on the chemical composition of fumarolic gases suggest that they are emitted from a hydrothermal-dominated system with shallow magmatic influence (Brombach et al. 2000; Villemant et al. 2014; Tamburello et al. 2019; Moretti et al. 2020a,b; Moune et al. 2022). At the surface, fluids are emitted from radial faults and fractures cutting the dome, such as Cratère Sud (CS; the site of the main fumarolic emissions) and 8 Juillet 1976 fractures (Fig. 1b), and open pits caused by past eruptions (for example Gouffre 56). The hot area surrounding fumarolic manifestations and fractures (particularly around Napoleon Nord and Gouffre 56; Fig. 1b) is progressively expanding, which has led to an increasing budget of heat flux and soil degassing (Jessop et al. 2021) and has contributed to the progressive degradation of vegetation. Other signs of strong hydrothermal activity are the low-deep (<2.5 km below the summit) seismic activity (reaching up to 3000 very low-magnitude volcano-tectonic events in November 2020; OVSG-IPGP 2020), the nearly radial pattern of the Global Navigation Satellite System (GNSS) displacement vectors on the dome and the radial opening (3-7 mm/year) of dome fractures at most hydrothermalized sites (Moretti et al. 2020a). As a result of all these elements, La Soufriere has a permanent status of increased vigilance (alert level is Yellow, the second on a scale of four), further reinforced after the 2018 episode of accelerated unrest (Moretti et al. 2020a).

Cratère Sud (CS) and Napoleon Nord (NapN) are the only fumaroles accessible for direct sampling at the summit. They are regularly sampled by the Observatoire Volcanologique and

Sismologique de la Guadeloupe (OVSG-IPGP). CS is hosted along the Cratère Sud fault and is formed of three main vents, Cratère Sud Nord, Cratère Sud Central, and Cratère Sud Sud (CSN, CSC, and CSS, respectively). Although they have shown, sporadic variable behavior since 1992, the chemical composition of fumarolic gases and outlet gas temperatures have remained very similar, if not the same, at the CSN and CSC vents since 2016 (Moretti et al. 2020; Moune et al. 2022), while CSS has not yet been surveyed by in situ techniques. The temperature at CS has fluctuated between 95 (the temperature of the saturated steam vapor at the summit atmospheric pressure) and 110 °C, but it reached 140 °C in 1999-2000 (Villemant et al. 2014). At NapN, a fumarole that emerged in 2014 in the hot expanding area, the temperature remained virtually stable at 95 °C (Moretti et al. 2020a). According to Moretti et al. (2020a), temperature increases are primarily associated with the input of deep magmatic gases into the hydrothermal system, whereas temperature drops and the restoring of the saturated steam temperature may be favored by interaction with very shallow groundwater and then be influenced by external forces such as heavy rain (average of 5 m/year in the 2017-2020 period; OVSG-IPGP bulletins) or wetter seasons (Moune et al. 2022). CS is characterized by jet-type fumarolic emissions, abundant deposition of native sulfur, and sporadic ejection of solid fragments, while NapN has weaker fumarolic emissions and restricted native sulfur deposition.

Periodic chemical analyses using soda bottles demonstrated that fumarolic gases are mixtures of steam, $CO_2$, and $H_2S$ (concentrations of 96-98, 1.5-4.0, and 0.3-0.7 mol%, respectively), in addition to minor concentrations (<0.03 mol%) of $N_2$, $CH_4$, He, and CO (Brombach et al. 2000; Moretti et al. 2020a). Such concentrations have remained stable since 2017, except for the March-June 2018 period where $CO_2$, gaseous sulfur species, CO, and He reached maximum concentrations associated with the arrival of deep anomalous "magmatic" gases and hotter fluids that perturbed the hydrothermal system (Moretti et al. 2020a; Moune et al. 2022). The chemical composition of fumarolic gases is controlled by variable scrubbing processes within hydrothermal aquifers, which efficiently removes $SO_2$ and $H_2S$ (Allard et al. 2014; Tamburello et al. 2019; Moretti et al. 2020a; Moune et al. 2022) to form native sulfur and sulfate/sulfide mineral assemblages (e.g., Giggenbach 1987; Symonds et al. 2001). Based on relative concentrations of $CO_2$, $H_2S$, and $SO_2$ measured in 2016-2020, previous studies (Tamburello et al. 2019; Moune et al. 2022) showed that at La Soufriere volcano, CS has a more magmatic-hydrothermal signature than NapN, responding quickly to any changes occurring in magmatic and hydrothermal sources. These studies suggested that NapN has been affected by major

scrubbing effects due to a localized cold, shallow aquifer that buffers fumarolic emissions both thermally and chemically (Tamburello et al. 2019).

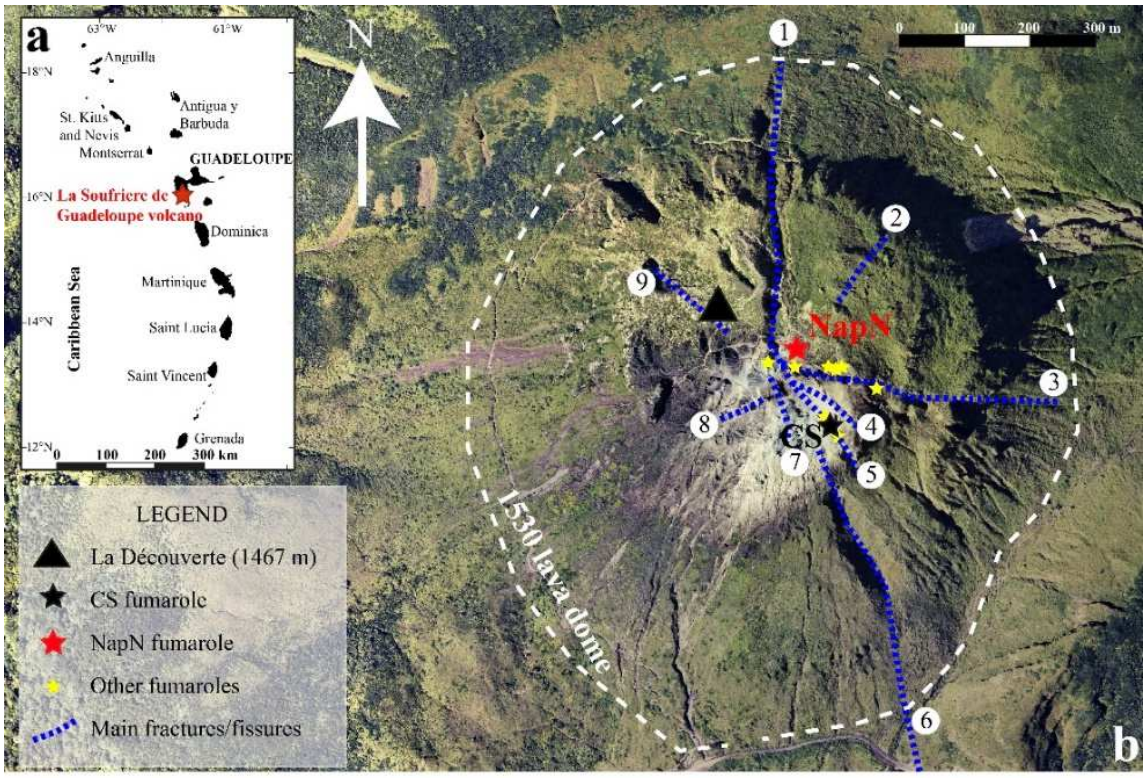


**Figure 1** a) Location of Guadeloupe island and La Soufriere volcano in the Lesser Antilles volcanic arc. b) Location of fumarolic emissions (yellow stars) and main fissures/fractures (blue dashed lines) within the 1530 lava dome. Positions of CS and NapN sites are shown as black and red stars, respectively, while the enclosed area shows the lava dome position. (1) Nord fracture, (2) Nord-Est fracture, (3) 8 Juillet 1976 fracture and Breislack fault, (4) Lacroix fracture, (5) Cratère Sud fracture, (6) 30 Août 1976 fracture and Faille de la Ty, (7) Gouffre Peyssonel, (8) Dolomieu fracture, (9) Nord-Ouest fracture

## 3. Sampling and analytical methods

Gas condensate (hereafter named condensates) samples were obtained using a 50 cm-long fiberglass tube used to channel flow from the fumarole, connected to a Pyrex-Dewar glass elbow. Sample collection followed the "normal" and "direct" procedures proposed by Chevrier and Le Guern (1982). The "normal" method connected a Pyrex-Dewar glass to a Pyrex coil condenser cooled with freshwater. The "direct" method replaced the coil condenser with a 20 cm-silicon tube. The "normal" method was used at the CS fumarole, while the "direct" method was generally used at NapN (Table 1). In-situ chemical analysis for chlorine performed on

samples collected simultaneously by the "direct" and "normal" methods showed no significant variations (e.g., Chevrier and Le Guern 1982). The outlet gas temperature was recorded at the end of the procedure. Subsequently, the sample was stored in polyethylene bottles and transported to the OVSG-IPGP laboratory for chemical analysis.

Ion chromatography (IC; Dionex Aquion™, Thermo Scientific) analyses were conducted at the OVSG-IPGP chemistry laboratory, usually within a week of the sampling to determine the concentration of chloride and sulfate in unfiltered samples. 100 µL of sample diluted by 100 were used for IC analyses, while the remaining solution was hermetically stored at ambient temperature in a dry, cool place until used for analysis of trace elements. Measurements were achieved following internal analysis protocols and regular calibration routines. The analytical error was ≤5%. Then, 2 to 10 mL of condensates were filtered using syringes and 0.20 µm pore-size sterile cellulose filters (VWR, number 514-0061), and transported to the laboratories at the IPGP (Paris, France) in acidified (with 0.05 mL of $HNO_3$, 67-69%, Fisher Chemical, A467-250) polyethylene bottles. These samples were analyzed by Inductively Coupled Plasma Mass Spectrometry (ICP-MS; Agilent 7900) to obtain the concentrations of major and trace elements. Furthermore, rock samples with minor hydrothermal alteration (23CF and SOU-J4) from the 1530 lava dome and scoria fallout deposits collected by Boudon et al. (2008) and Metcalfe et al. (2021), respectively, were selected and analyzed once again in this study for major and trace elements using the ICP-MS technique. Internal standards for condensate samples (e.g., Sc, In, Re), international standards (e.g., BEN, BIR-1, BHVO-2, BCR-2, ATHO-1, LIP, RGM-1) for rock analyses, and blank solutions were used to control possible error sources and validate results. The analytical error for condensate and rock analyses was generally <10%.

Nine samples that contained noticeable black and white/yellow particles were filtered using 0.45 µm pore-size nitrocellulose filters (Millipore, CAS 9004-70-0) and then analyzed by Scanning Electron Microscope (SEM, Quanta 250) in the C3-Mag laboratory at the Université des Antilles (Pointe-à-Pitre, Guadeloupe). First, the sample was shaken, and then 5-8 mL were poured into a funnel-shaped plastic container where the liquid phase drained and particles were trapped on the nitrocellulose filter. The filters with particles were then dried for 24 hours at 50 °C. Before analysis, filters were cut into ~8x8 mm squares and mounted on carbon tape-covered aluminum holders. High-resolution imaging was retrieved using the back-scattered electron (BSE) mode, while semi-quantitative chemical analyses were performed in the EDS

mode using an acceleration voltage of 15 kV, beam current of 5 nA, 15-40 s dwell time, and 10 mm working distance. Acquisition of high-resolution images and data processing were carried out using the INCAEnergy® software.

# 4. Results

## 4.1 Microscopic observations in condensates

Condensate samples displayed from a range from a few to abundant small particles, solid precipitates in the inner walls of polyethylene bottles, and clear to cloudy appearance (Table 1). As shown in Table 1, particles were common in the condensates; they were observed in 53 of the 55 samples studied. Samples with black and white, or just white particles, were predominant, while a few samples displayed only black particles. CS samples showed a larger number of particles and a much cloudier aspect than NapN samples. In general terms, samples with a moderate to abundant number of particles had a cloudy to milky aspect, while samples with a limited presence of particles had a predominantly clear aspect. It is important to note that samples collected before April 2019 for CS and before July 2019 for NapN displayed a predominantly clear aspect with minor to moderate amounts of particles, while cloudy to milky samples predominated from mid-2019 in both CS and NapN samples.

**Table 1** Color, abundance, and appearance of condensates. Samples with solid crusts in the inner parts of bottles and samples selected for SEM-EDS analyses were highlighted. Sample appearance reflects the degree of turbidity of the sample, the sample being "clear" with no turbidity (colorless, like water), "slightly cloudy" for those samples with noticeable turbidity, and "milky" for those samples with significant turbidity (like milk). B&W: black and white particles. N/A: Not applicable/Not analyzed.

| Sample | Date | Site | Prescence of particles | Color | Abundance | Appearance | Solid precipitates | Submitted to microscopic analyses? |
|---|---|---|---|---|---|---|---|---|
| C1 | 11/04/2017 | CSC | yes | B&W | abundant | slightly cloudy | no | N/A |
| C2 | 08/06/2017 | CSC | yes | B&W | few particles | slightly cloudy | no | N/A |
| C3 | 25/07/2017 | CSC | yes | white | few particles | clear | yes | N/A |
| C4 | 24/11/2017 | CSC | no | N/A | N/A | clear | no | N/A |
| C5 | 24/11/2017 | CSC | yes | black | few particles | clear | no | N/A |
| C6 | 31/01/2018 | CSC | yes | white | few particles | clear | no | N/A |
| C7 | 19/04/2018 | CSC | yes | white | abundant | clear | yes | N/A |
| C8 | 02/05/2018 | CSN | yes | white | few particles | clear | no | N/A |
| C9 | 02/06/2018 | CSC | yes | B&W | few particles | clear | no | N/A |
| C10 | 30/07/2018 | CSC | yes | white | few particles | clear | no | N/A |
| C11 | 11/09/2018 | CSC | yes | white | abundant | slightly cloudy | yes | N/A |
| C12 | 24/10/2018 | CSC | yes | B&W | few particles | slightly cloudy | no | N/A |
| C13 | 22/11/2018 | CSC | yes | white | middle | slightly cloudy | no | yes |

| | | | | | | | | |
|---|---|---|---|---|---|---|---|---|
| C14 | 19/12/2018 | CSC | yes | white | middle | clear | yes | yes |
| C15 | 22/01/2019 | CSC | yes | B&W | middle | clear | no | N/A |
| C16 | 22/03/2019 | CSC | yes | B&W | middle | clear | yes | N/A |
| C17 | 30/04/2019 | CSC | yes | B&W | few particles | clear | no | N/A |
| C18 | 11/06/2019 | CSC | yes | B&W | abundant | slightly cloudy | yes | yes |
| C19 | 14/07/2019 | CSC | yes | white | abundant | slightly cloudy | no | yes |
| C20 | 03/09/2019 | CSC | yes | B&W | abundant | slightly cloudy | yes | N/A |
| C21 | 01/10/2019 | CSC | yes | N/A | N/A | slightly cloudy | no | N/A |
| C22 | 08/10/2019 | CSN | yes | B&W | middle | clear | no | N/A |
| C23 | 05/12/2019 | CSN | yes | B&W | middle | slightly cloudy | yes | N/A |
| C24 | 27/02/2020 | CSC | yes | white | few particles | clear | yes | N/A |
| C25 | 10/04/2020 | CSC | yes | white | few particles | slightly cloudy | yes | N/A |
| C26 | 15/05/2020 | CSC | yes | white | abundant | slightly cloudy | yes | N/A |
| C27 | 18/06/2020 | CSC | yes | white | abundant | slightly cloudy | no | N/A |
| C28 | 05/08/2020 | CSC | yes | B&W | abundant | slightly cloudy | no | N/A |
| C29 | 08/10/2020 | CSC | yes | B&W | middle | clear | no | N/A |
| C30 | 08/10/2020 | CSC | yes | B&W | middle | slightly cloudy | yes | N/A |
| C31 | 23/11/2020 | CSC | yes | white | abundant | milky | yes | N/A |
| C32 | 23/11/2020 | CSC | yes | B&W | abundant | slightly cloudy | no | N/A |
| C33 | 08/12/2020 | CSC | yes | B&W | middle | milky | no | yes |
| C34 | 16/01/2021 | CSC | yes | white | middle | milky | yes | N/A |
| C35 | 16/01/2021 | CSC | yes | white | abundant | milky | yes | N/A |
| C36 | 11/04/2017 | NapN | yes | B&W | few particles | clear | no | yes |
| C37 | 08/06/2017 | NapN | yes | B&W | few particles | clear | no | N/A |
| C38 | 25/07/2017 | NapN | yes | black | middle | clear | no | N/A |
| C39 | 30/07/2018 | NapN | no | N/A | N/A | clear | no | N/A |
| C40 | 24/10/2018 | NapN | yes | white | few particles | clear | no | N/A |
| C41 | 19/12/2018 | NapN | yes | white | few particles | clear | no | N/A |
| C42 | 22/01/2019 | NapN | yes | white | few particles | clear | no | N/A |
| C43 | 19/02/2019 | NapN | yes | B&W | middle | clear | no | N/A |
| C44 | 22/03/2019 | NapN | yes | B&W | middle | clear | no | N/A |
| C45 | 11/06/2019 | NapN | yes | white | middle | clear | no | yes |
| C46 | 14/07/2019 | NapN | yes | B&W | few particles | clear | no | N/A |
| C47 | 03/09/2019 | NapN | yes | B&W | middle | slightly cloudy | no | yes |
| C48 | 01/10/2019 | NapN | yes | white | abundant | slightly cloudy | no | yes |
| C49 | 08/10/2019 | NapN | yes | B&W | few particles | clear | no | N/A |
| C50 | 05/12/2019 | NapN | yes | B&W | few particles | clear | no | N/A |
| C51 | 27/02/2020 | NapN | yes | B&W | few particles | slightly cloudy | no | N/A |
| C52 | 10/04/2020 | NapN | yes | black | few particles | slightly cloudy | no | N/A |
| C53 | 05/08/2020 | NapN | yes | B&W | abundant | slightly cloudy | no | N/A |
| C54 | 08/10/2020 | NapN | yes | B&W | few particles | clear | no | N/A |
| C55 | 08/12/2020 | NapN | yes | B&W | few particles | slightly cloudy | yes | N/A |

N/A: Not applicable/Not analyzed

## 4.2 Microscopic SEM-EDS observations

After filtration of nine condensate solutions, 177 EDS analyses (Supplementary Material 1) and SEM-BSE observations (Fig. 2) were performed, and they allowed us to identify four distinct types of solid particles (Fig 4, Table 2):

1) Rock particles. Subrounded- to angular-shaped particles whose size varied from a few micrometers up to ~140 µm. These particles were Si-rich, with significant concentrations of rock-related elements (i.e., K, Mg, Ca, Ti, Fe; Fig. 2a). These fragments were the most abundant and common in condensates, especially at NapN

(Fig. 3). They were eroded from the fumarolic conduit, as proven by previous works focused on volcanic aerosols (e.g., Aiuppa et al. 2003; Martin et al. 2008).

2) S-bearing particles. Subrounded to subangular particles of ≤110 μm diameter containing significant amounts of S (Fig. 2b). The highest S concentrations (up to 100 wt.%) were ascribed to the presence of amorphous and crystalline native sulfur (Fig. 2b), while lower values were attributed to the presence of sulfates (Supplementary Material 1). These particles predominated in CS condensates (Fig. 3), while only three were found in NapN samples. The origin of solid S-particles could be ascribed to sulfur precipitation during the condensation process (Fischer et al. 1998) and/or emission in the aerosol phase (e.g., Moune et al. 2010; Calabrese and D'Alessandro 2015), the latter being trapped during the condensation process.

3) Cl-bearing particles. Subrounded- to subangular-shaped particles of <50 μm in diameter (Fig. 2d) and occasionally translucent in appearance. These particles had significant concentrations of Cl (by up to 37.8 wt.%), together with Na, K, Ca, and Fe. In general terms, all Cl-containing SEM-EDS spectrums were considered within this group, except for those point analyses which displayed a low Cl concentration (<4 wt.%) and significant concentrations (>10 wt.%) of Si. Nine Cl-bearing particles were found at CS, while only two were found at NapN. These particles were commonly found in the aerosol phase within volcanic plumes (e.g., Obenholzner et al. 2003; Moune et al. 2010; Mandon et al. 2019).

4) Si-rich spherules. Small (<10 μm) rounded particles formed by Si and O. These particles appeared in both NapN and CS samples (Fig. 2e). However, only four-point analyses (Supplementary Material 1) enabled them to be identified due to their small size. Therefore, the number of Si-rich particles could be greatly underestimated. The origin of Si-rich microspherules in volcanic systems has been commonly associated with bubbles bursting at the magma air interface (Martin et al. 2008) or leaching of glass fragments by acidic gases (e.g., Spadaro et al. 2002; Moune et al. 2007). However, given the low temperature of fumarolic emissions at La Soufriere, Si-rich particles appear to be related to A-opal precipitation which occurs commonly in geothermal systems (Garcia-Valles et al. 2008; Peng and Jones 2012).

**Table 2** Summary of the physicochemical characteristics of the solid particles identified within condensate samples. Detailed information is presented in Supplementary Material 1.

| Fragment Type | Rock particles | S-bearing particles | Cl-bearing particles | Si-rich particles |
|---|---|---|---|---|
| **Occurrence** | Common | Occasional | Occasional | Rare |
| **Morphology** | Subrounded to angular. Usually, they formed agglutinates | Subrounded to subangular. Presence of agglutinates of sulfur in CS | Subrounded to subangular | Spherical/ Rounded |
| **Size** | <140 µm | <110 µm | <50 µm | <10 µm |
| **Chemical composition** | Main: Si, O<br>Minor: Fe, Ti, Ca, Zr, Al, K, Ca | Main: S, O<br>Minor: Si | Main: O, Cl, Na, K<br>Minor: Si, S, Ca | Main: Si, O |
| **Mineral phases** | - | Native sulfur<br>Na-Ca sulfates | Possible halite<br>Fe-Chlorides | Amorphous silica |

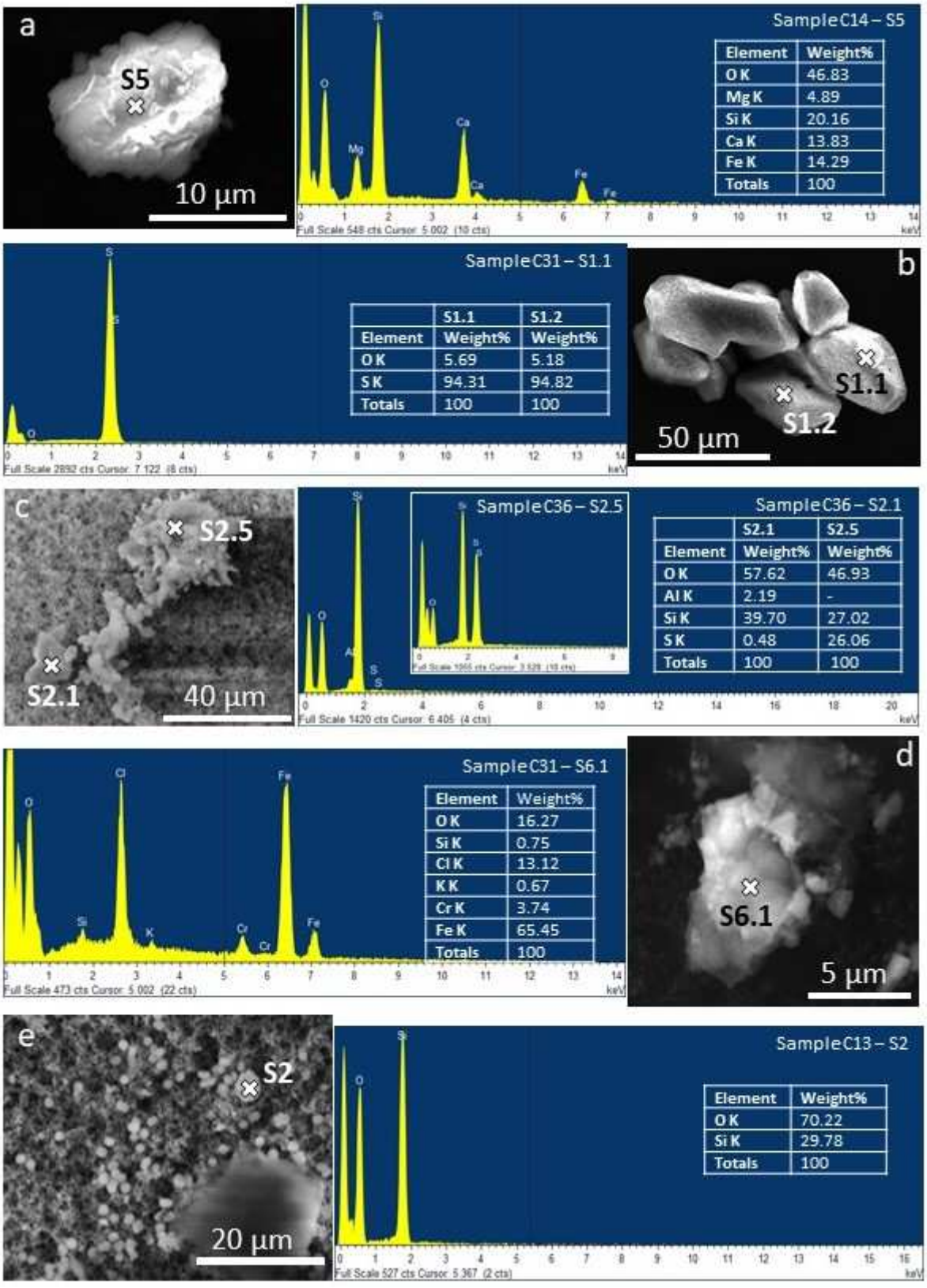


296

297 **Figure 2** Physicochemical characteristics of the solid particles found in condensates: a) rock
298 particles that contained variable concentrations of rock-forming elements (i.e., K, Mg, Ca, Ti,
299 Fe); b) rhombic native sulfur particles; c) agglutinate of Si particles with variable

concentrations of rock-forming elements and sulfur; d) Cl-bearing particle with alkaline, earth-alkaline, and Fe as main ligand elements; e) small round/spheroidal particles that contained Si and O. Sample codes were listed in Table 1. White crosses represent EDS analyses, whose spectrums (S) are included in Supplementary Material 1. Tables within spectrums display normalized wt.% values.

Rock particles were dominant in condensates, followed by S-bearing and Cl-bearing compounds (Fig. 3). Conversely, Si-rich spherules were less common. However, three sources of uncertainty could bias the particle count: i) only a modest fraction of samples (9 out of 55 samples) were studied by the SEM-EDS technique, ii) for each sample, not all particles were analyzed, either due to their similar appearance, their small size that produced significant background noise, or a working/measuring strategy that was focused on the identification of particles that displayed different signal intensities, iii) presence of agglutinates (Fig. 2c) composed of rock- and S-bearing particles that were considered as single fragments. Consequently, the particle count (Fig. 3) was underrated and should not be taken as strictly significant to provide sample statistics. However, independent of the possible biased particle count, two clear tendencies can be distinguished in Fig. 3: 1) the amount of rock particles is greater at NapN than CS, and 2) S- and Cl-bearing particles are predominant at CS. We can thus anticipate that the tendencies suggest a significant erosive contribution in NapN condensates during the study period.

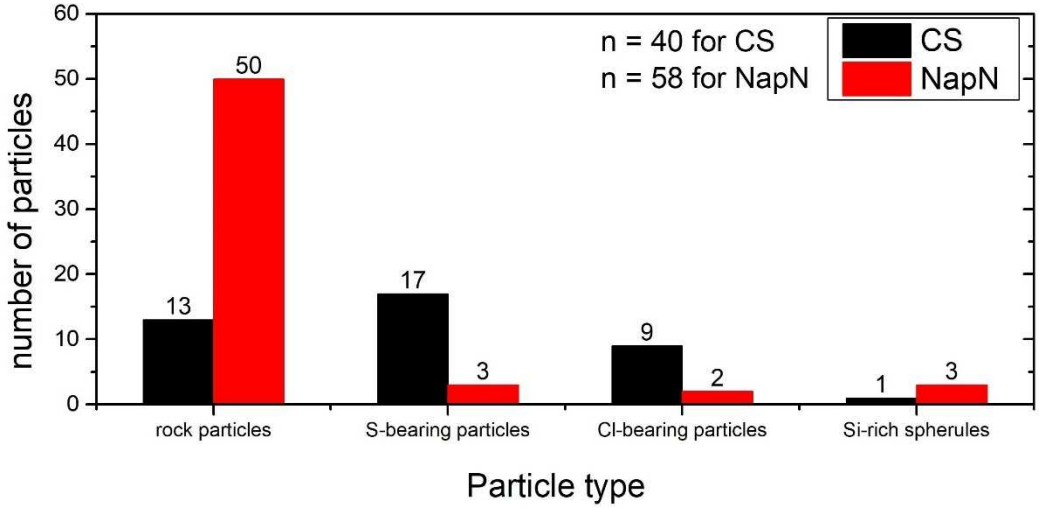


**Figure 3** Histograms of the amount and type of particles within condensate samples. A total of 98 particles were identified based on 177 SEM-EDS analyses (Supplementary Material 1, column "Z") and considered for this plot. However, this number of particles is an was

underestimate given that not all of them were analyzed (see text to further details). Black and red bars represent CS and NapN samples, respectively.

### 4.3 Physicochemical characteristics of condensates

Outlet gas temperature of analyzed samples, pH, and concentrations of $Cl^-$ and $SO_4^{2-}$ of condensates collected from CS and NapN fumaroles are presented in Table 3. The outlet gas temperatures at CS varied from 95 to 108.4 °C, with maximum values in April 2018, November 2019, and January 2021 samples (Fig. 4b). Over the same period, NapN temperatures remained within the narrow range of 94.4±0.9 °C (Fig. 4b). In the same way as for the outlet gas temperature, CS samples also recorded greater pH variations (ranging from 0.92 to 4.52) than NapN samples (between 2.70 and 3.41). These pH variations (Fig. 4a) agreed with those found in worldwide volcanoes (values from ~0 to 4.5; Gemmell 1987, Taran et al. 1995; Africano and Bernard 2000; Chaplygin et al. 2016) and coincided with pH values (between 1.1 and 5) obtained during the 1976 phreatic explosions at La Soufriere (Chevrier and Le Guern 1982). The lowest pH values (~1) at CS were comparable with those condensates measured in high-temperature magmatic systems as Kudryavy (Russia) or San Cristobal (Nicaragua) volcanoes (Gemmell 1987; Taran et al. 1995).

The concentration of $Cl^-$ in CS and NapN (Table 3) was within the range of 0.9 to 4798 mg/L and 0.2 to 42.4 mg/L, respectively. Cl contents showed a roughly positive correlation with outlet gas temperature in the case of CS and a negative correlation with pH (Fig. 4). Sulfate concentrations for CS and NapN ranged from 2.0 to 573.9 mg/L and 2.2 to 80.8 mg/L, respectively. No correlation was found between sulfate concentrations (Table 3) and the amount of particles or sample aspect (Table 1), suggesting that the variable presence of particles is more related to mechanical processes (i.e., vent erosion) than to the chemical composition of condensates. Chlorine concentrations measured in CS and NapN agree with those condensates collected during the 1976 phreatic explosions at Col de l'Echelle (Chevrier and Le Guern 1982). However, samples collected since July 2019 at CS have exhibited a notable increase in $Cl^-$ concentration, the highest recorded at La Soufriere fumaroles (Fig. 4c, Table 3). On the other hand, sulfate contents showed variable concentrations (Table 3), but they did not correlate with the outlet gas temperature nor the pH of condensates.

**Table 3** Fumarolic site, pH, outlet gas temperature (in °C) of analyzed samples, condensation procedure, and concentrations (mg/L) of $Cl^-$ and $SO_4^{2-}$ in condensate samples.

| | Date | Site | pH | Temp °C | Method | $Cl^-$ mg/L | $SO_4^{2-}$ mg/L |
|---|---|---|---|---|---|---|---|
| C1 | 11/04/2017 | CSC | 3.68 | 95.9 | Normal | 2.4 | 18.2 |
| C2 | 08/06/2017 | CSC | 3.68 | 95.4 | Normal | 2.5 | 19.0 |
| C3 | 25/07/2017 | CSC | 4.00 | 98.9 | Normal | 2.5 | 8.4 |
| C4 | 24/11/2017 | CSC | N/A | 98.9 | Normal | 7.6 | 22.0 |
| C5 | 24/11/2017 | CSC | 3.50 | 98.9 | Normal | 1.7 | 9.5 |
| C6 | 31/01/2018 | CSC | 3.86 | 100.2 | Normal | 5.1 | 23.9 |
| C7 | 19/04/2018 | CSC | 2.63 | 104.2 | Normal | 73.9 | 5.9 |
| C8 | 02/05/2018 | CSN | 2.22 | 95.3 | Normal | 8.0 | 138.6 |
| C9 | 02/06/2018 | CSC | 3.79 | 95 | Normal | 1.3 | 4.2 |
| C10 | 30/07/2018 | CSC | 4.29 | 95.3 | Normal | 4.7 | 17.4 |
| C11 | 11/09/2018 | CSC | 2.68 | 101 | Normal | 0.9 | 14.9 |
| C12 | 24/10/2018 | CSC | 3.83 | 95.2 | Normal | 1.1 | 2.0 |
| C13 | 22/11/2018 | CSC | 4.52 | 95.2 | Normal | 2.3 | 10.9 |
| C14 | 19/12/2018 | CSC | 3.21 | 100.1 | Normal | 1.8 | 26.1 |
| C15 | 22/01/2019 | CSC | 2.30 | 100 | Normal | 2.5 | 563.6 |
| C16 | 22/03/2019 | CSC | 3.32 | 98.5 | Normal | 2.7 | 4.0 |
| C17 | 30/04/2019 | CSC | 3.95 | 95 | Normal | 2.4 | 38.7 |
| C18 | 11/06/2019 | CSC | 2.79 | 96.3 | Normal | 6.0 | 573.9 |
| C19 | 14/07/2019 | CSC | 2.28 | 102.8 | Normal | 135.8 | 15.1 |
| C20 | 03/09/2019 | CSC | 1.88 | >99.8 | Normal | 593.5 | 22.3 |
| C21 | 01/10/2019 | CSC | 1.85 | 105.6 | Normal | 663.0 | 3.9 |
| C22 | 08/10/2019 | CSN | 1.58 | 108.2 | Normal | 1206.0 | 30.0 |
| C23 | 05/12/2019 | CSN | 2.51 | 105.6 | Normal | 51.2 | 2.9 |
| C24 | 27/02/2020 | CSC | 2.96 | 99.1 | Normal | 28.3 | 227.4 |
| C25 | 10/04/2020 | CSC | 2.53 | 103.4 | Normal | 62.6 | 4.6 |
| C26 | 15/05/2020 | CSC | 1.81 | 101.1 | Normal | 449.1 | 5.1 |
| C27 | 18/06/2020 | CSC | 1.98 | 99.5 | Normal | 483.3 | 8.8 |
| C28 | 05/08/2020 | CSC | 2.10 | 101.8 | Normal | 332.0 | 8.1 |
| C29 | 08/10/2020 | CSC | 3.13 | 98.9 | Normal | 21.3 | 2.3 |
| C30 | 08/10/2020 | CSC | 3.21 | 98.9 | Normal | 20.3 | 5.3 |
| C31 | 23/11/2020 | CSC | 1.12 | 107.2 | Normal | 2858.2 | 10.1 |
| C32 | 23/11/2020 | CSC | 0.92 | 107.2 | Normal | 4505.0 | 14.1 |
| C33 | 08/12/2020 | CSC | 1.33 | 106 | Normal | 1690.5 | 9.1 |
| C34 | 16/01/2021 | CSC | 0.98 | 108.4 | Normal | 4129.5 | 23.6 |
| C35 | 16/01/2021 | CSC | 1.00 | 108.4 | normal | 3562.0 | 46.0 |
| C36 | 11/04/2017 | NapN | 3.41 | 94.8 | Direct | 0.5 | 2.2 |
| C37 | 08/06/2017 | NapN | 3.36 | 94.7 | Direct | 2.0 | 6.5 |
| C38 | 25/07/2017 | NapN | 3.19 | 94.8 | Direct | 4.8 | 49.1 |
| C39 | 30/07/2018 | NapN | 3.2 | 95.1 | N/A | N/A | N/A |
| C40 | 24/10/2018 | NapN | 3.01 | 95 | N/A | 0.9 | 2.5 |
| C41 | 19/12/2018 | NapN | 3.21 | 95 | Direct | 0.3 | 9.1 |
| C42 | 22/01/2019 | NapN | 3.00 | 95 | Direct | 0.3 | 6.4 |
| C43 | 19/02/2019 | NapN | 2.89 | 95.1 | Direct | 0.2 | 3.6 |
| C44 | 22/03/2019 | NapN | 3.31 | 95.1 | Direct | 42.4 | 3.9 |
| C45 | 11/06/2019 | NapN | 3.23 | 93.5 | Direct | 10.4 | 67.1 |
| C46 | 14/07/2019 | NapN | 3.21 | 94.1 | Direct | 2.0 | 3.7 |
| C47 | 03/09/2019 | NapN | 3.22 | 94.8 | Direct | 1.3 | 20.6 |
| C48 | 01/10/2019 | NapN | 3.25 | 95.3 | Normal | 7.2 | 14.9 |
| C49 | 08/10/2019 | NapN | 2.94 | 95.1 | Normal | 17.9 | 37.1 |
| C50 | 05/12/2019 | NapN | 2.70 | 95.2 | Direct | 3.9 | 80.8 |
| C51 | 27/02/2020 | NapN | 3.20 | 95 | Direct | 1.6 | 30.4 |
| C52 | 10/04/2020 | NapN | 3.11 | 95 | Direct | 10.0 | 8.6 |
| C53 | 05/08/2020 | NapN | 3.34 | 95 | Direct | 0.6 | 6.7 |
| C54 | 08/10/2020 | NapN | 3.24 | 94.9 | Direct | 0.5 | 9.7 |
| C55 | 08/12/2020 | NapN | 2.96 | N/A | Direct | 0.2 | 13.8 |

354 N/A: Not applicable/Not analyzed

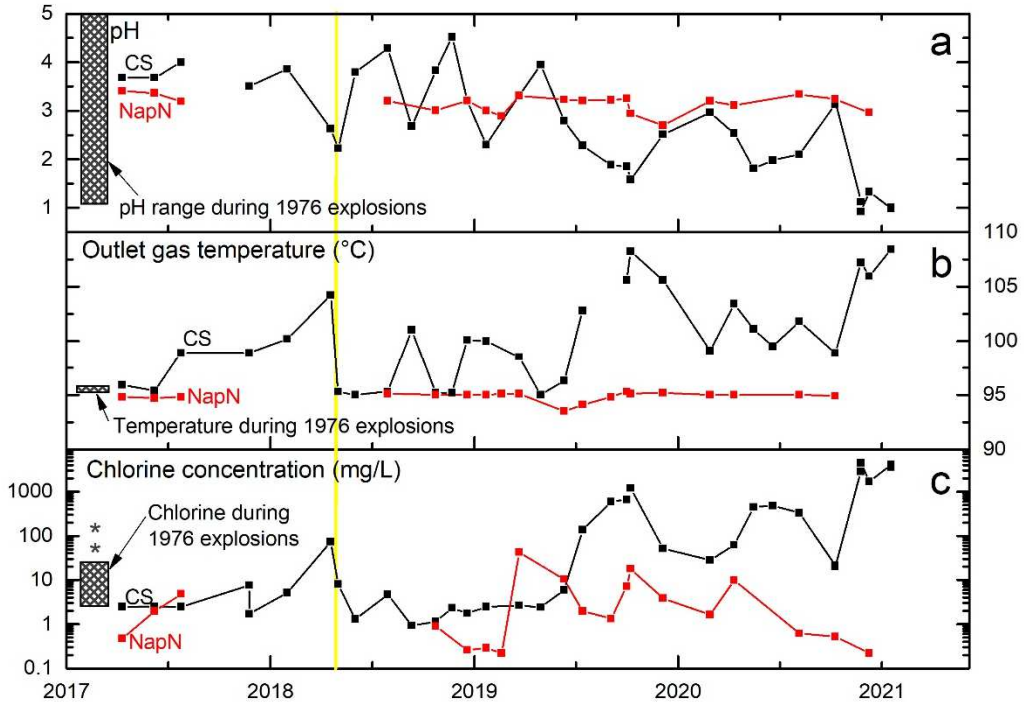


355

356 **Figure 4** Physicochemical variations in a) pH, b) outlet gas temperature, and c) chlorine
357 concentration in CS (black lines) and NapN (red lines) samples during the study period. Dashed
358 areas show pH, outlet gas temperature, and Cl concentrations obtained for samples collected
359 during the July-August 1976 explosions at Col de l'Echelle (Chevrier and Le Guern 1982).
360 Asterisks in panel (c) show two outlier chlorine concentrations measured for the 1976
361 eruptions. The yellow line shows the earthquake of $M_L$ 4.1 on April 27, 2018, which was felt
362 by the population.

363 ### 4.4 Trace element concentrations in condensate samples

364 Corrected concentrations (in ppb) of major and trace elements for representative samples are
365 presented in Table 4, while complete data including analytical dilution factors, blank
366 corrections, and %RSD (Relative Standard Deviation) values are provided in Supplementary
367 Material 2. Chemical element concentrations displayed great dispersion, as demonstrated by
368 significant percentile variation coefficients (49 and 393%) in both CS and NapN, likely
369 attributed to variations in outlet gas temperatures, steam fluxes, or the variable chemical
370 composition of fumarolic emissions. Of the studied chemical elements, 41.6% exhibit median
371 RSD <10%, while 81% showed median RSD values <50%. The lowest %RSD was associated
372 with abundant chemical elements (Cl and S), some alkali and earth-alkali elements (Mg, K, Ca,
373 Rb, Sr, Cs, Ba), transition metals (V, Cr, Mn, Fe, Co, Ni, Cu, Zn, Y) and other metal and

metalloid elements (B, Al, Si, Sb). Various lithophile (Li, Na, Ti, Br, Zr, U, and Rare Earth Elements; REEs), chalcophile (Ag, Cd, Sn), and siderophile (Mo, Sn) elements had slightly higher median %RSD (between 10 and 50%), while As and I had medium-high %RSD (median around 50%). Be, Tl, Bi, and Th reached the highest median %RSD (usually >100%), mainly due to their very low (generally <0.1 ppb) concentrations.

Condensates were mainly composed of Si, S, and Cl, representing 23-99.9% and 50-99.8% of the total concentration of condensates in CS and NapN samples, respectively. Therefore, trace elements occasionally represented a small fraction in analyzed samples. Sulfur, Cl, and rock-forming elements (such as Na, Mg, Al, Si, or Ca) had high concentrations in condensates (Table 4), with values of between $10^1$ and $10^7$ ppb. Metal and metalloid elements (i.e., Cr, Co, Ni, Zn, As, Ag, Cd) had concentrations ranging from $10^{-1}$ to $10^2$ ppb, apart from Fe and Zn, which reached concentrations in the order of $10^3$-$10^4$ ppb, like rock-related elements. REEs generally showed concentrations <1 ppb (Table 4). By comparing condensate samples collected on the same date at CS and NapN (Fig. 5), the average concentrations at NapN samples were often higher than those of CS samples, except for Li, B, Cl, Zr, Mo, Ag, Sb, Pb, Bi, and U. This pattern could result from the minor proportion of condensed steam in NapN compared to CS (75 mol% versus 96 mol% of steam, respectively, e.g., Tamburello et al. 2019; Moretti et al. 2020a), thus yielding lower degrees of dilution of collected samples and therefore higher concentrations of elements (e.g., Gemmell 1987). Gas/steam ratios from CS presented in Moretti et al. (2020), OVSG monthly reports (http://www.ipgp.fr/fr/ovsg/bulletins-mensuels-de-lovsg), and Brombach et al. (2000) showed slight variations (ranging from 0.018 to 0.058, with an average of 0.032) between 2017 and 2021, while they reached a maximum value (0.099) in June 2018 when degassing was markedly perturbed (e.g., Moretti et al. 2020a). Also, the proportion of steam found in CS using Giggenbach ampoules (96-97 mol%; Moretti et al. 2020a) agrees with MultiGas data (96 mol%) measured by Tamburello et al. (2019) in 2016. Regrettably, there is no published data from Giggenbach ampoules at NapN. Therefore, previously collected data from CS show that the proportion of steam remained constant during this study period. Similarly, based on the behavior of CS, it is believed that NapN maintained a constant proportion of steam during the study period.

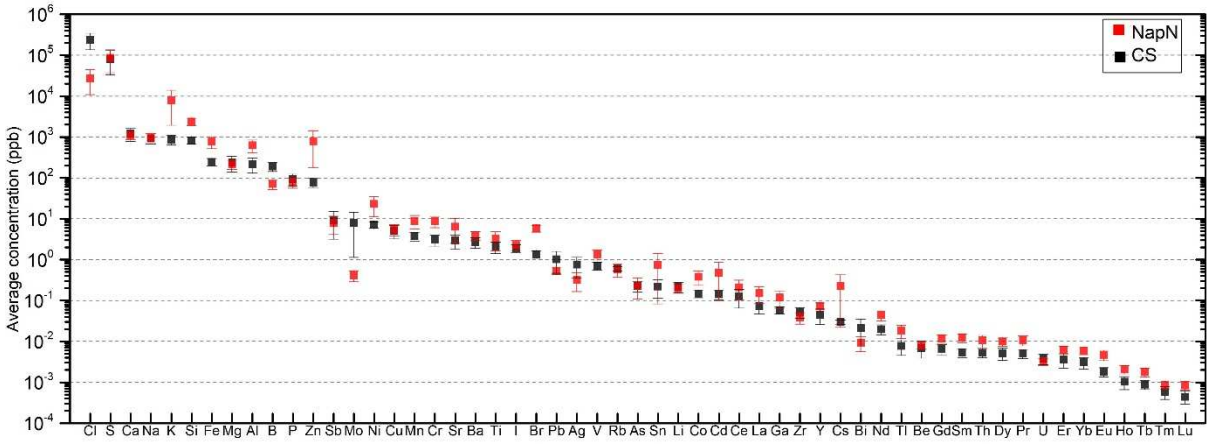


403

404 **Figure 5** Average concentration (in ppb) of condensates collected on the same dates from CS
405 (black squares) and NapN (red squares) fumaroles. For example, concentrations of samples
406 collected between mid-2017 and mid-2018 were not considered, given that NapN was not
407 sampled in that period. Bars represent the standard error of the mean.

408 Notable chemical variations were depicted at CS and NapN (Fig. 6), even for the most abundant
409 elements with high confidence (with low %RSD). Concentrations above baseline values of
410 several chemical elements (e.g., S, Si, Na, B) were observed in the CS sample collected in May
411 2018 and associated with the volcanic unrest described by Moretti et al. (2020a), with values
412 up to four orders of magnitude above average (for instance, S and Na; Fig. 6; Table 4).
413 Similarly, CS samples frequently showed greater concentrations at the end of 2020 and the
414 beginning of 2021. It is important to note that B and Cl concentrations at CS (Fig. 6) showed a
415 generally incremental pattern over the study period. Conversely, chemical elements at NapN
416 tended to reach higher concentrations during the second half of 2019. The uniformly disparate
417 behavior between CS and NapN suggested variable physicochemical processes that affected
418 the feeding source of these emissions.

419 **Table 4** Concentration (in ppb) of major and trace elements in representative condensates
420 collected between April 2017 and January 2021 from CS and NapN fumaroles. Complete data
421 and Weigh Ash Fraction percentages (%WAF; See Appendix B for further details) are
422 presented in Supplementary Material 2. <blk: below detection limit.

| **Sample** | **C-3** | **C-8** | **C-18** | **C-35** | **C-38** | **C-46** | **C-55** | **WAF%** | **WAF%** |
|---|---|---|---|---|---|---|---|---|---|
| **Date** | **25/07/2017** | **02/05/2018** | **11/06/2019** | **16/01/2021** | **25/07/2017** | **14/07/2019** | **08/12/2020** | **average** | **average** |
| **Fumarole** | **CS** | **CS** | **CS** | **CS** | **NapN** | **NapN** | **NapN** | **CSC** | **NapN** |
| Li | 0.170 | 4.243 | 0.366 | 0.284 | 0.623 | 0.056 | 0.143 | 23.4 | 36.2 |
| Be | 0.0065 | 0.0471 | 0.0003 | 0.0168 | 0.0123 | 0.0028 | 0.0019 | 39.3 | 56.4 |
| B | 10.24 | 5593.84 | 77.14 | 1721.76 | 15.04 | 23.01 | 72.87 | 0.08 | 0.70 |

| | | | | | | | | | |
|---|---|---|---|---|---|---|---|---|---|
| Na | 757.48 | 32393671 | 932.48 | 1038.46 | 501.93 | 65.09 | 1230.81 | 100 | 100 |
| Mg | 93.67 | 4.61 | 85.34 | 245.52 | 474.78 | 39.55 | 127.21 | 100 | 100 |
| Al | 175.67 | 3807.70 | 186.90 | 192.12 | 2532.46 | 28.18 | 119.73 | 100 | 100 |
| Si | 573.84 | 122398.81 | 876.39 | 3962.99 | 5111.39 | 3670.77 | 356.54 | 100 | 100 |
| P | 214.83 | 1792.21 | 94.96 | 21.69 | 314.17 | <blk | 22.38 | 100 | 100 |
| S | 15822 | 9534766 | 23229 | 1693274 | 14955 | 8484 | 6399 | 0.004 | 0.009 |
| Cl | 1869.1 | 4101.6 | 4842.1 | 3276623.2 | 4167.2 | 1053.4 | 1987.5 | 1.3 | 1.4 |
| K | 2161.2 | 3516.2 | 3951.3 | 359.4 | 3014.1 | 811.0 | 859.3 | 100 | 100 |
| Ca | 475.9 | 741.7 | 994.9 | 1617.2 | 1997.0 | 199.6 | 755.8 | 100 | 100 |
| Ti | 10.40 | 33.07 | 0.66 | 3.56 | 0.84 | 0.34 | 0.35 | 100 | 100 |
| V | 2.55 | 1.26 | 0.81 | 1.36 | 0.92 | 0.20 | 0.27 | 60.9 | 62.7 |
| Cr | 0.54 | 3.92 | 2.24 | 4.30 | 0.53 | 3.50 | 3.29 | 100 | 100 |
| Mn | 11.87 | 2.56 | 4.89 | 4.36 | 13.01 | 0.65 | 6.86 | 100 | 100 |
| Fe | 143.96 | 169.56 | 489.47 | 366.49 | 1248.10 | 59.30 | 269.10 | 100 | 100 |
| Co | 0.33 | 1.12 | 0.12 | 0.53 | 0.14 | 0.05 | 0.32 | 45.9 | 48.6 |
| Ni | 20.95 | 2.27 | 5.92 | 19.47 | 4.84 | 1.89 | 9.49 | 0.9 | 1.7 |
| Cu | 4.77 | 1.63 | 1.90 | 5.39 | 3.25 | 0.68 | 0.55 | 9.3 | 13.6 |
| Zn | 95.94 | 13.38 | 171.89 | 721.02 | 36.66 | 27.64 | 212.85 | 0.4 | 0.6 |
| Ga | 0.118 | 0.486 | 0.090 | 0.098 | 0.127 | 0.007 | 0.020 | 71.7 | 82.3 |
| As | 0.147 | 3.054 | 0.183 | 2.150 | <blk | 0.042 | <blk | 2.6 | 21.3 |
| Br | 2.16 | 4.27 | 2.09 | 2.75 | 21.87 | 1.04 | 1.66 | 0.4 | 0.2 |
| Rb | 0.18 | 3.14 | 0.38 | 0.95 | 0.44 | 0.03 | 1.14 | 100 | 100 |
| Sr | 1.24 | 54.42 | 2.55 | 2.52 | 6.65 | 0.30 | 1.54 | 100 | 100 |
| Y | 0.019 | 0.048 | 0.035 | 0.063 | 0.128 | 0.008 | 0.051 | 100 | 100 |
| Zr | 0.02 | 32.16 | 0.03 | 0.55 | 0.01 | <blk | <blk | 100 | 100 |
| Mo | 5.48 | 57.29 | 0.07 | 0.22 | 0.06 | 0.05 | <blk | 1.3 | 4.9 |
| Ag | 0.132 | 0.016 | 6.348 | 0.108 | 0.020 | 1.225 | <blk | 4.5 | 8.6 |
| Cd | 0.114 | 0.056 | 0.310 | 0.254 | 0.066 | 0.008 | 0.355 | 0.9 | 1.5 |
| Sn | 0.007 | 0.154 | 0.017 | 0.623 | 0.007 | <blk | 0.003 | 20.9 | 57.3 |
| Sb | 3.46 | 3.84 | <blk | 7.41 | 2.55 | 3.27 | 3.40 | 0.19 | 0.06 |
| I | <blk | 130.63 | 1.42 | 21.15 | <blk | 1.08 | <blk | 2.6 | 11.5 |
| Cs | 0.04 | 3.41 | 0.02 | 0.02 | 0.07 | 0.00 | 0.01 | 100 | 100 |
| Ba | 4.33 | 11.76 | 3.75 | 5.42 | 17.13 | 0.62 | 1.19 | 100 | 100 |
| La | 0.04960 | 0.00460 | 0.05447 | 0.05619 | 0.88457 | 0.00552 | 0.06143 | 100 | 100 |
| Ce | 0.03884 | 0.03948 | 0.09101 | 0.08580 | 0.61679 | 0.00165 | 0.08392 | 100 | 100 |
| Pr | 0.00155 | 0.00392 | 0.00633 | 0.00745 | 0.03037 | 0.00050 | 0.00395 | 100 | 100 |
| Nd | 0.00767 | 0.01448 | 0.02504 | 0.03357 | 0.11957 | 0.00184 | 0.01961 | 100 | 100 |
| Sm | 0.00165 | 0.02524 | 0.00743 | 0.01080 | 0.02706 | 0.00041 | 0.00925 | 100 | 100 |
| Eu | 0.00161 | 0.00383 | 0.00184 | 0.00271 | 0.01866 | 0.00019 | 0.00162 | 100 | 100 |
| Gd | 0.01433 | 0.00065 | 0.00632 | 0.01185 | 0.02493 | <blk | 0.00520 | 100 | 100 |
| Tb | 0.00033 | 0.00107 | 0.00111 | 0.00126 | 0.00409 | 0.00022 | 0.00132 | 100 | 100 |
| Dy | 0.00208 | 0.00293 | 0.00576 | 0.00619 | 0.02252 | 0.00058 | 0.00731 | 100 | 100 |
| Ho | 0.00034 | 0.00911 | 0.00126 | 0.00113 | 0.00424 | 0.00000 | 0.00096 | 100 | 100 |
| Er | 0.00089 | 0.00301 | 0.00301 | 0.00399 | 0.01238 | 0.00017 | 0.00470 | 100 | 100 |
| Tm | 0.00033 | 0.00115 | 0.00051 | 0.00076 | 0.00167 | 0.00018 | 0.00064 | 100 | 100 |
| Yb | 0.00116 | 0.00739 | 0.00391 | 0.00458 | 0.01159 | 0.00103 | 0.00471 | 100 | 100 |
| Lu | 0.00012 | 0.00180 | 0.00042 | 0.00028 | 0.00183 | 0.00006 | 0.00052 | 100 | 100 |
| Tl | <blk | 0.07 | 0.01 | <blk | <blk | <blk | <blk | 9.0 | 6.3 |
| Pb | 0.19 | 0.64 | 0.92 | 6.11 | 0.41 | 0.12 | 0.72 | 2.0 | 4.6 |
| Bi | 0.0023 | 0.0579 | 0.0131 | 0.0288 | 0.0021 | 0.0052 | 0.0013 | 0.1 | 0.7 |
| Th | 0.0053 | <blk | 0.0016 | <blk | 0.0056 | <blk | <blk | 100 | 100 |
| U | 0.0009 | 0.0927 | 0.0033 | 0.0061 | 0.0039 | 0.0002 | 0.0019 | 100 | 100 |

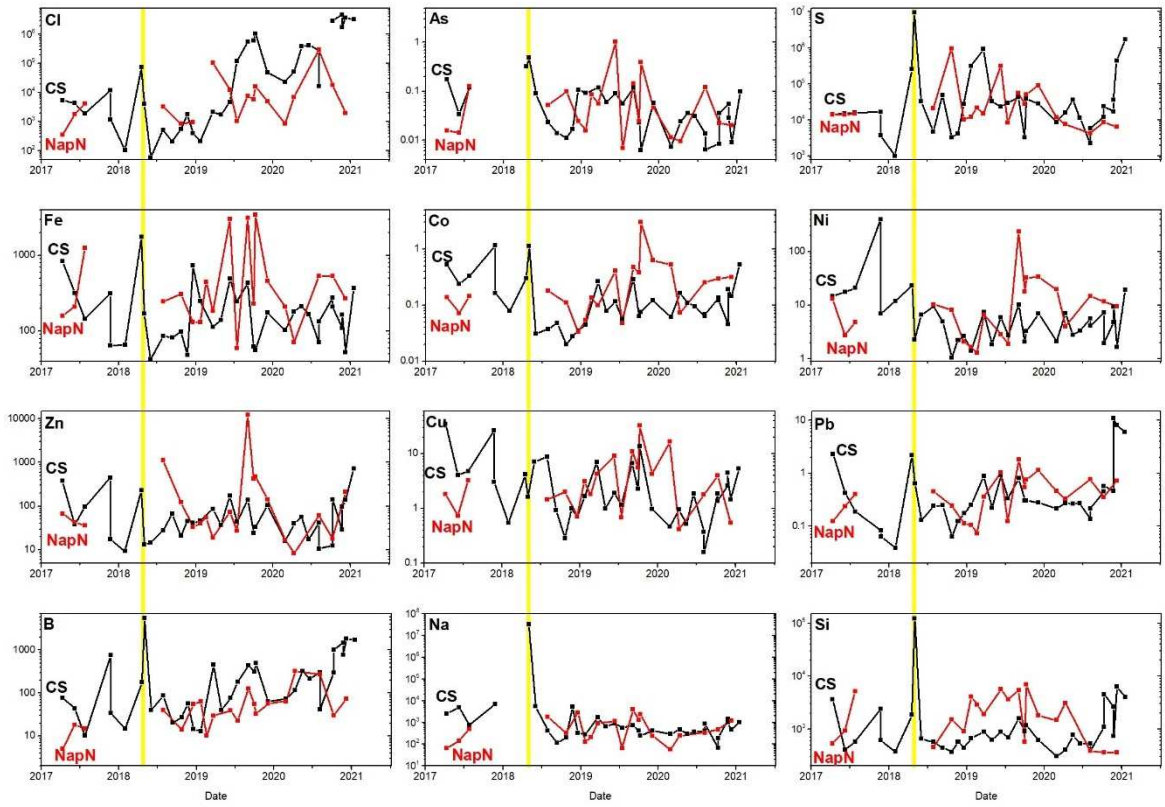


**Figure 6** Long-term variations in the concentration of representative chemical elements during the period from May 2017 to January 2021. Samples from CS and NapN have a distinct and constant dilution factor during the study period. The yellow line shows the earthquake ($M_L$ 4.1) on April 27, 2018. Black and red lines represent CS and NapN fumaroles, respectively.

# 5. Discussion

## 5.1 Representativity of samples

IC and ICP-MS techniques are frequently used to characterize the chemical composition of a wide variety of solid or liquid samples. While the IC technique offers fast and practical measurements of major ions dissolved in liquid samples, the ICP-MS technique offers accurate and precise measurements for chemical elements in trace and ultra-trace (<1 ppm) concentrations. In this work, chlorine and sulfur contents (in the form of sulfates in the case of IC technique) were measured by both IC and ICP-MS methods, allowing the results to be compared and their representativeness evaluated. Despite a few outliers, there was a good general agreement between the two techniques for chlorine concentration determination for both CS and NapN samples (Fig. 7a). On the other hand, the sulfur contents in CS and NapN samples showed a large dispersion, with no a clear correlation between the two techniques (Fig.

7b). It is well known that suppressed or enhanced signals could be obtained in ICP-MS analyses on high ionic strength solutions due to the precipitation of salts on the nebulizer or the presence of high concentrations of matrix elements such as $H_2SO_4$ (Fischer et al. 1998; Nelms 2005). Fig. 7 shows that the large inconsistencies between the two methods were beyond the analytical error of each technique. Greater chlorine and sulfur concentrations in ICP-MS than IC analyses suggest the presence of other Cl- and S-compounds that were not analyzed by the IC technique. This mismatch was common in the case of sulfur (Fig. 7b), where species such as $SO_3^{2-}$, $HSO_4^-$, $S^{2-}$ can be found (Africano and Bernard 2000). Based on these assumptions, discrepancies in S content by both techniques could be explained by the presence of unknown S-species, in agreement with typically higher S concentrations measured by ICP-MS than IC (Fig. 7b).

The presence of solid particles (Fig. 3) could modify the original chemical composition of condensate samples since re-equilibration processes related to dissolution and/or precipitation of solid phases could occur within the acid solution, especially in those samples stored for a longer time (up to four years) and with lower pH. Indeed, dissolution processes could explain the higher Cl and S concentrations measured by the ICP-MS technique (Fig. 7). Dissolution of Cl-bearing particles is feasible given the hydrophilic behavior of Cl (Africano and Bernard 2000), which could explain the small number of Cl-bearing particles detected on SEM analyses (Fig. 3). Similarly, dissolution processes could efficiently remove lithophile and siderophile elements by leaching of rock particles (Taran et al. 1995; Symonds et al. 1996). Therefore, dissolution of Cl-bearing and rock particles should increase the concentration of siderophile and lithophile elements in samples. On the other hand, the dissolution of S compounds is not expected since it can only occur in the presence of hot aqua regia.

Precipitation of S-bearing compounds has been previously documented for condensate samples (Fischer et al. 1998). Sulfur precipitation in aqueous solutions typically occurs when $SO_4^{2-}$ concentrations are above ~1000 mg/L (e.g., Fischer et al. 1998), while precipitation of sulfur and sulfate minerals (e.g., gypsum, anhydrite, barite) from highly charged acid waters in crater lakes (natural analog of condensates) has been documented when $SO_4^{2-}$ concentrations are above 10,000 mg/L (e.g., Agusto et al. 2016; Inguaggiato et al. 2018, Mandon et al. 2020). Such $SO_4^{2-}$ concentrations are higher than those found in La Soufriere's condensates ($\leq$574 mg/L, Table 3), therefore we infer negligible sulfur precipitation in the latter. Consequently, sulfur crusts found inside polyethylene bottles could be due to the decantation of suspended matter instead of precipitation processes. Therefore, trace element sequestration from the

aqueous solution was discarded, as documented in previous works focusing on sulfur precipitates (e.g., Fischer et al. 1998). In the case of amorphous silica precipitates, significant amounts of lithophile elements, in addition to Fe, As, and Sb, could be removed from the solution (Reyes et al. 2002; Sanchez-Yañez et al. 2017). However, such chemical elements were not identified during the analysis of A-opal spherules.

Although dilution and precipitation processes affecting S- and Cl-bearing particles cannot be ruled out, it is believed that secondary re-equilibration processes only affected Si-particles. Moreover, the time-dependent test (Appendix A) demonstrated negligible exchange processes during a 67-day storage time (Fig. A1), although they did not take into account more extended periods nor trace elements which might have disguised clues about their behavior during longer storage times. Data dispersion associated with Cl and S contents mainly corresponded to i) analytical uncertainties when concentrations were below 10 ppm for Cl, and ii) presence of unanalyzed and unknown S-species, besides solid sulfur microparticles that caused interference with the measurement of sulfate concentrations (e.g., Fig. A1). Such analytical uncertainties become significant when concentrations are closer to the instrumental detection limits (e.g., 0.1 and 1 ppm for Cl and S in ICP-MS measurements, respectively) as depicted for Cl concentrations in Fig. 7a. Consequently, the data from the ICP-MS technique seems to be more reliable because i) analyses were done on filtered samples which minimized the noise caused by the presence of particles, and ii) ICP-MS carried out direct measurements of the total concentration for Cl and S. Therefore, data from this technique were used for computations in the following section.

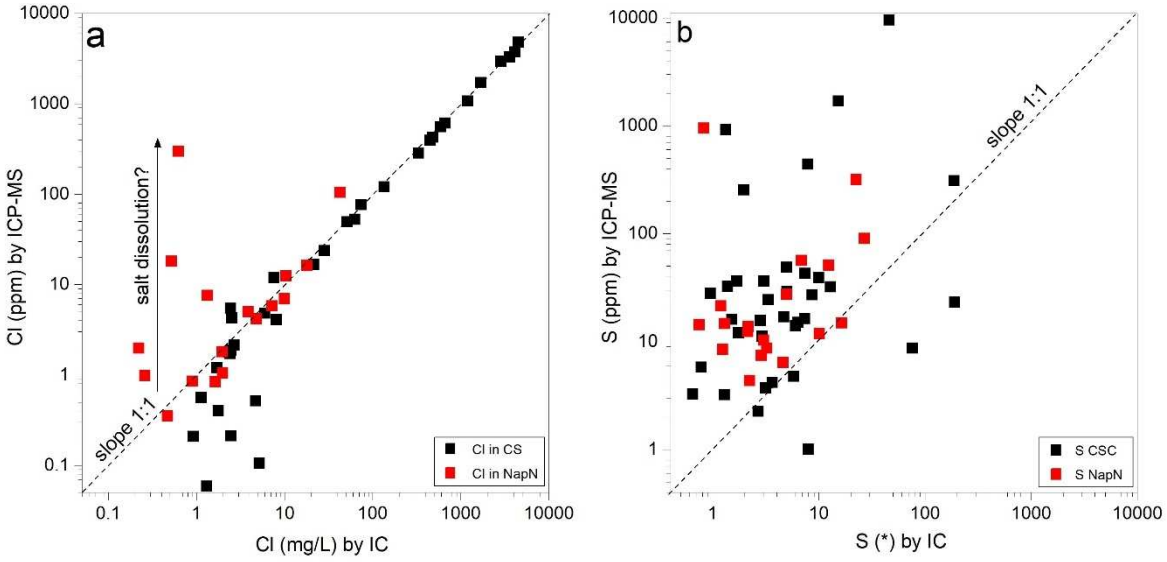

**Figure 7** Comparison between the concentration of (a) Cl and (b) S from both CS and NapN fumaroles, determined by ion chromatography (IC) and Inductively Coupled Plasma Mass Spectrometry (ICP-MS) techniques. It is important to note that IC analyses were performed within a week of sampling, while ICP-MS were carried out from a few months to up to four years after sampling. Black and red symbols represent CS and NapN samples, respectively. Dashed lines show the 1:1 ratio. S(*) corresponds to the molar concentration of sulfur in $SO_4$ alone.

## 5.2 Trace element volatility

Volcanic exhalations release volatile species and aerosols (e.g., Taran et al. 1995; Aiuppa et al. 2003; Mather et al. 2003), both mostly trapped during the condensation process. In general terms, erosion of host rock and hydrothermally altered fragments scavenged from the conduit walls has been ascribed as the primary process that contributes solid particles to condensate samples (e.g., Mather et al. 2003). Similarly, the transport of small aqueous particles (i.e., tiny droplets containing major and trace elements) becomes considerable in low-temperature steam-rich fumarolic emissions (e.g., Pokrovski et al. 2013; Censi et al. 2017). The erosive contribution can be accounted for based on the concentration of rock-related refractory elements (Gauthier and Le Cloarec 1998; Aiuppa et al. 2003; Gauthier et al. 2016). At La Soufriere, chondrite-normalized values (Fig. B.1) proved that REEs have been removed from host rocks, while typical rock-related elements (i.e., Al, Ti, Mn, Ca, Fe, Sr, Si, Zr, Na, K, P, Mg, Cr, Rb, Y, Cs, Ba, U, Th) are equally considered as a product of water-rock interaction within the hydrothermal system (Appendix B). Consequently, this work considers that Al, Ti, Mn, Ca, Fe, Sr, Si, Zr, Na, K, P, Mg, Cr, Rb, Y, Cs, Ba, REEs, U, and Th were transported as solids or within aqueous microparticles since they have a non-volatile behavior in the low-temperature emissions at La Soufriere volcano. Rock-related elements (including REEs) were removed following the weigh ash fraction approach (e.g., Aiuppa et al. 2003) presented in Appendix B.

### *5.2.1 Calculation of enrichment factors*

The relative volatility of trace elements has traditionally been estimated using the enrichment factor (EF; Duce et al. 1975; Mroz and Zoeller 1975), which measures the extent of enrichment (or depletion) of an element X in the condensate ($X_{cond}$) compared to whole rocks (e.g., Symonds et al. 1990; Africano and Bernard 2000; Zelenski et al. 2013, 2014; Chaplygin et al. 2015, 2016; Aguilera et al. 2016; Taran et al. 2018) following Eq. 1:

$$EF = (X/Y)_{cond}/(X/Y)_{rock} \quad \text{(Eq. 1)}$$

Where X is the element of interest and Y is the reference element in both the condensate (*cond*) and host rock (*rock*). The choice of the reference element is critical; normally, a trace element of low-moderate volatility present in low abundance levels in lavas is selected (Moune et al. 2010; Gauthier et al. 2016). Magnesium was used for normalization in previous studies on condensate samples obtained from volcanic systems at magmatic temperatures (Symonds et al. 1990; Zelesnki et al. 2013, 2014; Chaplygin et al. 2016; Taran et al. 2018). However, in the presence of active hydrothermal systems and low-temperature fumarolic emissions, Mg cannot be used as a reference element since it is related more to the leaching of host rocks than deep magmatic degassing. Therefore, cobalt was chosen as the reference element due to its low volatility and mobility in low-temperature hydrothermal systems (e.g., Scher et al. 2013) and low concentration in condensates (Table 4) and host rocks (Table 5). In addition, the re-equilibration processes during storage time for Co is considered as being insignificant since, to our knowledge, Co does not form secondary minerals, and its leaching from host rocks is limited (e.g., Scher et al. 2013). Co was also chosen because it presented low RSD percentages (Supplementary Material 2) and a large amount of data were available in our database for EF computations.

Co-based EFs are presented in Supplementary Material 3, and average values for CS and NapN computed with ash-corrected concentrations (Appendix B; Supplementary Material 3) are plotted in Fig. 8a. Theoretically, elements with EFs >1 were emitted mainly in a volatile form, while elements with EFs ≤1 were emitted in the solid phase (Zelenski et al. 2013). However, this paper considers that elements with EFs >1 were also transported as aqueous particles for a better understanding. Average log EF values ranged from -1 for Ga in NapN to 4.6 for S in CS. Sulfur, Sb, B, Cl, Bi, Br, Zn, Mo, Ni, Ag, Cd, As, I, and Pb showed a high to moderate volatile behavior, whereas Tl, Cu, Sn, Li, Be, Co, V, and Ga showed a poorly volatile behavior (Fig. 8a). In general terms, EFs for highly to moderately volatile elements were 9.2% (average) higher in CS than NapN, suggesting slightly higher volatility in CS samples likely due to CS having higher outlet gas temperatures (Fig. 4b) and fewer thermal and chemical scrubbing processes than NapN (e.g., Tamburello et al. 2019). Superior scrubbing at NapN would also be responsible for the decreased EFs of more soluble elements such as B, Cl, I, and As, as well as Bi, Mo, Pb, Tl, Li, and Ga. On the contrary, Br and Sn showed slightly higher EFs in NapN compared to CS. Despite such minor discrepancies, both fumarolic sites showed a similar

559 decreasing volatility pattern from S to Ga, implying a similar transport mode of each element
560 in CS and NapN.

561 S and Sb had the highest volatile behavior in La Soufriere fumaroles (Fig. 8a) with the highest
562 average EFs (log EFs between 3.8 and 4.6), followed by B, which reached an average log EF
563 of 3.3 and 2.7 in CS and NapN, respectively. Sulfur is a common constituent of volcanic
564 exhalations, and their high EFs agree with the presence of S-bearing particles in condensates
565 and S-rich fumarolic deposits around fumaroles. Likewise, it was supposed that most of the
566 sulfur collected in condensates was released as $H_2S$ (emission rates up to 3.5 ton/day in CSC;
567 Allard et al. 2014; Tamburello et al. 2019; Moune et al. 2022) and, to a lesser extent as $SO_2$.
568 Nevertheless, $H_2S$ is difficult to condense given its low solubility, whereas $SO_2$ is a minor
569 constituent at La Soufriere fumaroles despite its greater solubility. Therefore, EFs for sulfur
570 must be deeply underestimated given these condensation issues. Then, Sb and B had not been
571 previously reported in La Soufriere samples, though their higher EFs agreed with an expected
572 volatile behavior in low and high-temperature volcanic emissions (Symonds et al. 1990; Taran
573 et al. 2018; Mandon et al. 2020). Chlorine, Bi, Br, Zn, Mo, Ni, Ag, Cd, As, I, and Pb (in
574 decreasing order of volatility) showed moderate to low volatility with log EF values ranging
575 from ~1.5 to ~3.

576 **Table 5** Concentration (in ppm) of reference host rocks used to compute weight ash fractions
577 (WAF; Appendix B) and enrichment factors (EF; Supplementary Material 3). Samples 23CF
578 and SOU-J4 were selected due to their minimal hydrothermal alteration, and they correspond
579 to an andesite from the 1530 AD lava dome and a scoria fallout deposit from the 1657 eruption,
580 respectively. These samples had been previously analyzed for major and certain trace elements
581 by Boudon et al. (2008) and Metcalfe et al. (2021).

| | 23CF | SOU-J4 | Average | | 23CF | SOU J4 | Average |
|---|---|---|---|---|---|---|---|
| Li | 7.84 | 11.02 | 9.43 | La | 6.60 | 7.64 | 7.12 |
| Be | 0.56 | 0.69 | 0.62 | Ce | 15.75 | 17.98 | 16.86 |
| B | 21.35 | 24.77 | 23.06 | Pr | 2.01 | 2.31 | 2.16 |
| S | 241.00 | N/A | 241.00 | Nd | 9.80 | 10.52 | 10.16 |
| Cl | 8166 | 8250.1 | 8208.1 | Sm | 2.99 | 3.01 | 3.00 |
| V | 203.23 | 166.83 | 185.03 | Eu | 0.86 | 0.88 | 0.87 |
| Co | 24.55 | 20.37 | 22.46 | Gd | 3.10 | 3.28 | 3.19 |
| Ni | 18.19 | 9.74 | 13.96 | Tb | 0.58 | 0.58 | 0.58 |
| Cu | 81.25 | 44.56 | 62.91 | Dy | 3.60 | 3.77 | 3.68 |
| Zn | 62.12 | 57.52 | 59.82 | Ho | 0.80 | 0.77 | 0.78 |

| | | | | | | | |
|---|---|---|---|---|---|---|---|
| Ga | 16.00 | 15.93 | 15.97 | Er | 2.18 | 2.33 | 2.26 |
| As | 0.05 | 2.02 | 1.04 | Tm | 0.38 | 0.39 | 0.39 |
| Br | 1.62 | 0.69 | 1.15 | Yb | 2.30 | 2.49 | 2.40 |
| Mo | 0.65 | 0.75 | 0.70 | Lu | 0.38 | 0.37 | 0.37 |
| Ag | 0.07 | 0.06 | 0.06 | Tl | 0.067 | 0.16 | 0.11 |
| Cd | 0.15 | 0.08 | 0.11 | Pb | 2.34 | 2.82 | 2.58 |
| Sn | 0.90 | 2.05 | 1.48 | Bi | 0.0034 | N/A | 0.0034 |
| Sb | 0.07 | 0.13 | 0.10 | Th | 2.02 | 2.39 | 2.21 |
| I | 13.70 | 12.71 | 13.21 | U | 0.56 | 0.70 | 0.63 |

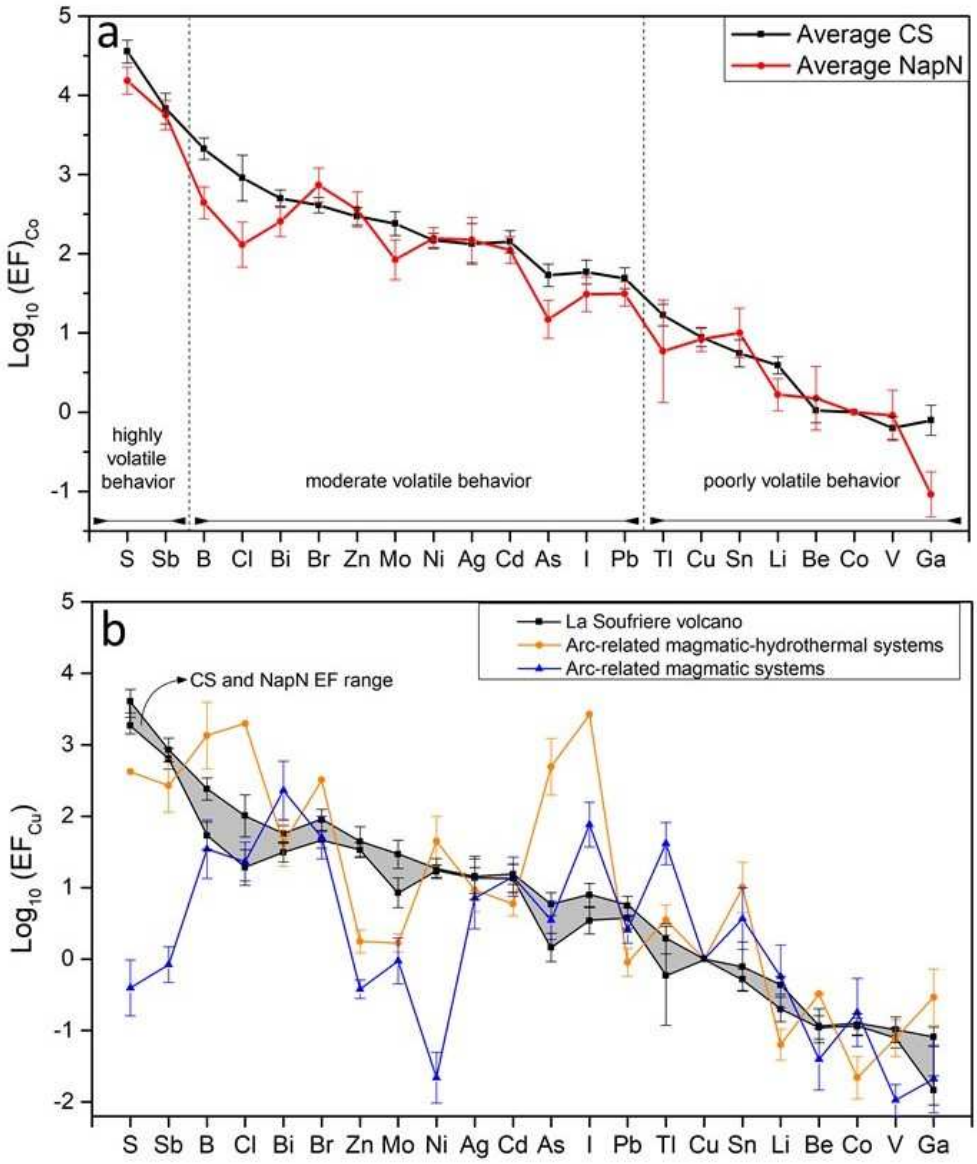


582

583 **Figure 8** Calculated enrichment factors (EF) for trace elements degassed at La Soufriere
584 volcano and comparison with other worldwide subduction-related volcanoes. a) Average Co-
585 based EFs for CS and NapN samples. b) Cu-based EFs estimated for comparison between La
586 Soufriere (grey area) and other arc-related volcanoes with trace element data in condensate

samples only. Magmatic-hydrothermal systems included Kawaj Ijen, Lastarria, and White Island volcanoes (Van Hinsberg et al. 2015; Aguilera et al. 2016; Mandon et al. 2020), while magmatic systems included Augustine, Kudryavy, Tolbachik, and Pallas volcanoes (Symonds et al. 1990; Taran et al. 1995, 2018; Chaplygin et al. 2016). EFs were recalculated (Supplementary Material 3) using Cu instead of Co or another lithophile element (e.g., Be, Mg) because Cu showed lower volatility at La Soufriere volcano (Fig. 8a) and usually presents poor to moderate volatility in volcanoes worldwide (e.g., Edmonds et al. 2018). Additionally, Cu was the trace element most commonly found in measurable concentrations at all the sites selected for comparison. Reference host rock concentrations for Augustine were taken from andesitic-to-dacitic ash fall deposits (Lepel et al. 1978; Rose et al. 1988; Kodosky and Keskinen 1990), and from basaltic-andesitic fall deposits for Kawaj Ijen (Handley et al. 2007; van Hinsberg et al. 2010). Volcanoes with average outlet gas temperatures greater than 450 °C were considered as magmatic systems, while volcanoes with lower temperatures (average discharge temperatures of 176, 328, and 408 °C for White Island, Lastarria, and Kawaj Ijen volcanoes, respectively; Supplementary Material 3) were classed as magmatic-hydrothermal systems (e.g., Aiuppa et al. 2017). Dashed vertical lines divide highly, moderate, and poorly volatile elements where the slope threshold was above 15%.

### *5.2.2 Comparison with other volcanoes*

Comparison of average EFs at La Soufriere and average EFs from other worldwide subduction-related volcanoes (Fig. 8b) enabled us to identify the different volatility behaviors of the trace elements collected using the same sampling technique. Despite some discrepancies, trace elements showed a general decrease in EF from the most (S) to the least (Ga) volatile element (Fig. 8b). EF patterns at La Soufriere are close to those of magmatic-hydrothermal systems, for which elements such as S, Sb, Bi, Ni, Ag, Cd, Pb, Tl, and Cu presented similar EFs, and therefore a similar behavior in terms of volatility. However, significant discrepancies were seen in B, Cl, As, Br, I, and Sn, which showed increased EFs in magmatic-hydrothermal volcanoes compared to La Soufriere volcano. Such discrepancies could be associated with the greater solubility of these elements where large hydrothermal reservoirs developed, such as at La Soufriere volcano, contrasting with magmatic-hydrothermal volcanoes characterized by less developed hydrothermal systems (e.g., Lastarria volcano; Aguilera et al. 2012). On the other hand, significantly higher EFs of S, Sb, Zn, Mo, Cd, and Pb were observed at La Soufriere relative to high-temperature magmatic systems. This could be ascribed to i) the greater volatility of these elements in emissions at lower outlet gas temperatures (<200°C; Quisefit et

al. 1989; Pokrovski et al. 2013; Mandon et al. 2020), ii) the greater volatility of Cu in magmatic systems that artificially lowered EFs from Eq. (1), or iii) the greater concentration of these elements in host rocks from magmatic subduction-related volcanoes relative to condensate samples (Supplementary material 3). Given the same geological context (i.e., subduction volcanoes), variations in the volatility of trace elements between La Soufriere and the other systems could likely be produced by different gas outlet temperatures and variable chemical composition fluid discharge as a result of variable fluid-rock interaction and scrubbing processes.

### *5.2.3 Temperature control, transport, and speciation of trace elements*

Periodic sampling carried out at the CS fumarole made it possible to investigate the behavior of lithophile, chalcophile, and siderophile elements against a background of varying temperature and chemical composition of the fumarolic emissions. In general, the concentration of chemical elements remained relatively stable as the temperature increased (Fig. 9). However, Cl displayed a faintly positive correlation with the outlet gas temperature, although with only a very low determination coefficient ($r^2$ of 0.50; Supplementary Material 4). Pb and Sn reached their maximum concentrations for temperatures above 106 °C (Fig. 9b, c), but these maxima concentrations did not follow any trend. Hence, it appears that the outlet gas temperature has a negligible effect on the chemical composition of the gas phase. A similar behavior was observed in magmatic systems (temperatures of between 585 and 940 °C for Kudryavy volcano; Taran et al. 1995; Symonds et al. 1996), where a slight increment in the concentration and volatility of certain species (e.g., Cl, I, Pb, As) as temperature increased was noted. At La Soufriere volcano, low outlet gas temperatures and the low-temperature range during the study period make it difficult to discuss the influence of temperature on the concentration of condensates in detail.

644 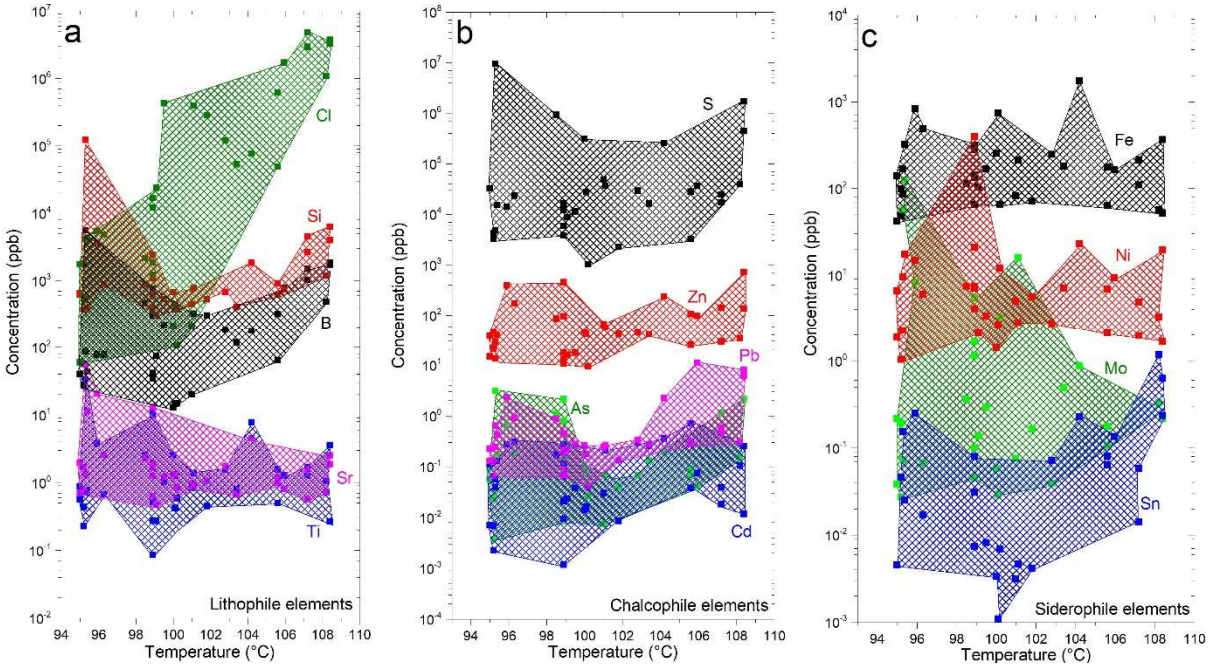


645 **Figure 9** Trace element concentrations of representative a) lithophile, b) chalcophile, and c)
646 siderophile elements in condensates versus outlet gas temperature at CS fumarole. Only
647 chemical elements with some degree of correlation with temperature (i.e., Cl from
648 Supplementary Material 4) and greater volatility behavior were plotted.

649 The transport and speciation of trace elements is usually accounted for using determination
650 coefficients (hereafter expressed as $r^2$) from linear correlations between common ligands (i.e.,
651 S, Cl, and Br) and selected major and trace elements (e.g., Crowe et al. 1987; Moune et al.
652 2006, 2010). Computed $r^2$ values (Supplementary Material 4) for NapN and CS were generally
653 low (average $r^2$ <0.37), using Cl, Br, and S as ligand elements. However, NapN fumarole had
654 $r^2$ values above 0.7 between Fe and some rock-forming elements such as Mg, Ca, and U, and
655 both NapN and CS exhibited $r^2$ values >0.5 between Fe and non-mobile trace elements,
656 including REEs. These higher correlation coefficients suggest that either at the source or during
657 transport, major and trace lithophile elements followed similar physicochemical processes
658 within the hydrothermal reservoir or fumarolic conduits. Leaching from host rocks and
659 subsequent transport to the surface as aqueous particles could explain the relationship between
660 Fe and lithophile elements in La Soufriere condensates. A deep magmatic source of lithophile
661 elements was discarded since they only show volatile behavior at high-temperature (>400 °C)
662 fumarolic emissions where lithophile elements are directly deposited from the gas phase (e.g.,
663 Taran et al. 2001; Africano et al. 2002; Henley and Seward 2018). Slightly higher
664 determination coefficients between Fe and lithophile elements at NapN compared to CS

(Supplementary Material 4) are ascribed to the incipient chemical dissolution of less hydrothermally altered host rocks deduced from the lower resistivity of rocks in the northern area of the dome where NapN is located (Rosas-Carbajal et al. 2016). The markedly larger amount of rock particles at NapN (Fig. 3) also supports the occurrence of erosive processes driven by high water-rock ratios within the fumarolic conduit. Low determination coefficients for halogens and sulfur suggest the enhanced transport of major and trace elements as solid and aqueous particles rather than halogen- and S-containing gaseous species, as typically occurs in magmatic and magmatic-hydrothermal volcanoes (e.g., Moune et al. 2010; Mandon et al. 2019; Scholtysik and Canil 2020). Consequently, the metals and metalloids plotted in Fig. 8a were mostly transported within tiny aqueous particles, following their low vapor/liquid partition coefficients at low temperatures and high boiling points which prevents their conversion to the gaseous phase in fumaroles at ~100 °C (e.g., Pokrovski et al. 2013). It is concluded that the enhanced transport of solid and aqueous particles is a specific characteristic of La Soufriere and suggests that this is a feature characterizing water-dominated fumarolic emissions in volcanic-hydrothermal systems.

## 6. Conclusions

This work provides the chemical composition of major and trace elements in condensate samples collected between April 2017 and January 2021 from two fumaroles (CS and NapN) at La Soufriere volcano, and is the first record of long-term trace element analyses in low-temperature (93.5 to 108.4 °C) fumarolic emissions. Despite low outlet gas temperatures, condensates contained significant amounts of siderophile, chalcophile, and lithophile elements. Such a broad contribution reflects the scavenging of chemical elements from magmatic and hydrothermal reservoirs. Furthermore, we found a faint positive correlation between Cl concentration, acidity of condensates, and outlet gas temperature at CS fumarole. At the same time, the low concentration of S in condensates from these emissions appeared to be underestimated given the problematic condensation of $H_2S$, which requires the use of other specialized techniques (e.g., alkaline traps) to obtain reliable S concentrations.

Compared to andesitic host rocks, condensates were enriched in S, Sb, B, Cl, Bi, Br, Zn, Mo, Ni, Ag, Cd, As, I, and Pb. Based on their physical properties (e.g., boiling temperature), it is believed that halogens and S were emitted as components of the gaseous phase. However, enrichments of Sb, Bi, Zn, Mo, Ni, Ag, Cd, As, and Pb were better explained through efficient transportation by tiny aqueous droplets, given their lower affinity with the vapor phase in low-

temperature emissions. Rock-related elements (including REEs) were present as solid particles, as shown by SEM analyses, as well as aqueous particles given their enhanced concentrations in filtered (<0.20µm) condensates.

Cu-based EFs suggest that the behavior of trace elements at La Soufriere volcano is comparable with other worldwide arc-related magmatic-hydrothermal systems such as Lastarria (Chile), Kawaj Ijen (Indonesia), and White-Island (New Zealand) volcanoes. However, some differences were noticed: i) a greater amount of rock-related elements in La Soufriere condensates, and ii) higher abundance of typically soluble species (mainly halogens) in magmatic-hydrothermal systems (i.e., volcanoes with magmatic influence but less developed hydrothermal systems) related to La Soufriere. The abundance of major and trace elements is likely controlled by the extent of the hydrothermal aquifer(s) (basically the water/rock ratio), their acidity and the pressure-temperature conditions that favor water-rock interaction in hydrothermal reservoirs. Our study demonstrates that the transport of chemical elements in low-temperature fumaroles is governed by the aerosol phase (except for noble gases, $N_2$, halogens, and related elements), and their abundances are linked with physicochemical processes taking place in hydrothermal reservoirs.

## Acknowledgments

We thank at the team of the Observatoire Volcanologique et Sismologique de la Guadeloupe (OVSG-IPGP) for helping to collect condensate samples and Pierre Burckel for performing ICP-MS analyses at the IPGP facilities. We also acknowledge Benoit Villemant (Institut des Sciences de la Terre de Paris, Sorbonne Université) and Abigail Metcalfe (IPGP) for providing reference samples of fresh unaltered rock and Benoit Caron (Institut des Sciences de la Terre de Paris, Sorbonne Universitè) for performing ICP-MS analyses of these rock samples. Special mention to Yves Bercion and Fabienne Zami from the C3 MAG laboratory at the Université des Antilles for assistance during SEM analyses.

## Funding statement

This work was supported by the EU-funded project IMMERGE (Impact multi-environnemental des retombées volcaniques et sahariennes en Guadeloupe) coordinated by C. Dessert (IPGP-UP). This project has been financially supported by European (FEDER FSE PO 2014-2020) and Région Guadeloupe funding (agreement GP0023419). This study contributes to the IdEx Université de Paris ANR-18-IDEX-XXXX and the Laboratory of excellence

ClerVolc number XXX. We thank IPGP for recurrent funding to the Observatoires Volcanologiques et Sismologiques (OVS-IPGP), the INSU-CNRS for funding provided by Service National d'Observation en Volcanologie (SNOV).

## Author contribution

**Manuel Inostroza:** Conceptualization, Methodology, Formal Analysis, Investigation, Data Curation, Writing – Original draft, Writing - Review and Editing, Visualization. **Séverine Moune**: Conceptualization, Methodology, Investigation, Resources, Writing - Review and Editing, Supervision, Project Administration. **Roberto Moretti**: Conceptualization, Validation, Writing – Review and Editing. **Magali Bonifacie**: Conceptualization, Investigation, Writing – Review and Editing. **Vincent Robert**: Methodology, Validation, Writing – Review and Editing. **Arnaud Burtin**: Methodology, Data Curation. **Elodie Chilin-Eusebe**: Methodology.

## Data Availability

Appendix A, B, and Supplementary Material xxxx can be found at XXXXXXXXXXXXXX

## References

Africano, F., Bernard, A., 2000. Acid alteration in the fumarolic environment of Usu volcano, Hokkaido, Japan. Journal of Volcanology and Geothermal Research, 97(1-4), 475-495.

Africano, F., Van Rompaey, G., Bernard, A., Le Guern, F. 2002. Deposition of trace elements from high temperature gases of Satsuma-Iwojima volcano. Earth, planets and space, 54(3), 275-286.

Aguilera, F., Layana, S., Rodríguez-Díaz, A., González, C., Cortés, J., Inostroza, M., 2016. Hydrothermal alteration, fumarolic deposits and fluids from Lastarria Volcanic Complex: A multidisciplinary study. Andean Geology, 43(2), 166-196.

Aiuppa, A., Dongarrà, G., Valenza, M., Federico, C., Pecoraino, G., 2003. Degassing of trace volatile metals during the 2001 eruption of Etna. Geophysical Monograph-American Geophysical Union, 139, 41-54.

Aiuppa, A., Fischer, T.P., Plank, T., Robidoux, P., Di Napoli, R., 2017. Along-arc, inter-arc and arc-to-arc variations in volcanic gas CO2/ST ratios reveal dual source of carbon in arc volcanism. Earth-Science Reviews, 168, 24-47.

Allard, P., Aiuppa, A., Beauducel, F., Gaudin, D., Di Napoli, R., Calabrese, S., Di Napoli, R., Crispi, O., Gaudin, D., Parello, F., Hammouya, G., Tamburello, G., 2014. Steam and gas emission rate from La Soufriere volcano, Guadeloupe (Lesser Antilles): implications for the magmatic supply during degassing unrest. Chemical Geology, 384, 76-93.

Allard, P., Aiuppa, A., Loyer, H., Carrot, F., Gaudry, A., Pinte, G., Michel. A., Dongarrà, G., 2000. Acid gas and metal emission rates during long-lived basalt degassing at Stromboli volcano. Geophysical Research Letters, 27(8), 1207-1210.

Boudon, G., Komorowski, J.C., Villemant, B., Semet, M.P., 2008. A new scenario for the last magmatic eruption of La Soufrière of Guadeloupe (Lesser Antilles) in 1530 AD Evidence from stratigraphy radiocarbon dating and magmatic evolution of erupted products. Journal of Volcanology and Geothermal Research, 178(3), 474-490.

Brombach, T., Marini, L., Hunziker, J.C. 2000. Geochemistry of the thermal springs and fumaroles of Basse-Terre Island, Guadeloupe, Lesser Antilles. Bulletin of Volcanology, 61(7), 477-490.

Calabrese, S., Aiuppa, A., Allard, P., Bagnato, E., Bellomo, S., Brusca, L., D'Alessandro, W., Parello, F. (2011). Atmospheric sources and sinks of volcanogenic elements in a basaltic volcano (Etna, Italy). Geochimica et Cosmochimica Acta, 75(23), 7401-7425.

Calabrese, S., D'Alessandro, W., 2015. Characterization of the Etna volcanic emissions through an active biomonitoring technique (moss-bags): Part 2–Morphological and mineralogical features. Chemosphere, 119, 1456-1464.

Censi, P., Inguaggiato, C., Chiavetta, S., Schembri, C., Sposito, F., Censi, V., Zuddas, P., 2017. The behaviour of zirconium, hafnium and rare earth elements during the crystallisation of halite and other salt minerals. Chemical Geology, 453, 80-91.

Chaplygin, I.V., Lavrushin, V.Y., Dubinina, E.O., Bychkova, Y.V., Inguaggiato, S., Yudovskaya, M.A., 2016. Geochemistry of volcanic gas at the 2012–13 New Tolbachik eruption, Kamchatka. Journal of Volcanology and Geothermal Research, 323, 186-193.

783 Chevrier, R.M., Le Guern, F., 1982. Prélèvement et analyses des condensats de fumerolles sur
784 volcans actifs: Soufrière de la Guadeloupe (1976–1977) et Pouzzoles et Vulcano (Italie)(1978).
785 Bulletin volcanologique, 45(3), 173-178.

786 Crowe, B.M., Finnegan, D.L., Zoller, W.H., Boynton, W.V. 1987. Trace element geochemistry
787 of volcanic gases and particles from 1983–1984 eruptive episodes of Kilauea volcano. Journal
788 of Geophysical Research: Solid Earth, 92(B13), 13708-13714.

789 Delmelle, P., Stix, J., Gases, J.V., 2000. Encyclopedia of volcanoes.

790 Duce, R.A., Hoffman, G.L., Zoller, W.H., 1975. Atmospheric trace metals at remote northern
791 and southern hemisphere sites: pollution or natural?. Science, 187(4171), 59-61.

792 Edmonds, M., Grattan, J., Michnowicz, S., 2015. Volcanic gases: silent killers. In Observing
793 the Volcano World (pp. 65-83). Springer, Cham.

794 Edmonds, M., Mather, T.A., Liu, E.J., 2018. A distinct metal fingerprint in arc volcanic
795 emissions. Nature Geoscience, 11(10), 790-794.

796 Fischer, T.P., Shuttleworth, S., O'Day, P.A., 1998. Determination of trace and platinum-group
797 elements in high ionic-strength volcanic fluids by sector-field inductively coupled plasma mass
798 spectrometry (ICP-MS). Fresenius' journal of analytical chemistry, 362(5), 457-464.

799 Garcia-Valles, M., Fernandez-Turiel, J.L., Gimeno-Torrente, D., Saavedra-Alonso, J.,
800 Martinez-Manent, S., 2008. Mineralogical characterization of silica sinters from the El Tatio
801 geothermal field, Chile. American Mineralogist, 93(8-9), 1373-1383.

802 Gauthier, P.J., Le Cloarec, M.F., 1998. Variability of alkali and heavy metal fluxes released by
803 Mt. Etna volcano, Sicily, between 1991 and 1995. Journal of Volcanology and Geothermal
804 Research, 81(3-4), 311-326.

805 Gauthier, P.J., Sigmarsson, O., Gouhier, M., Haddadi, B., Moune, S., 2016. Elevated gas flux
806 and trace metal degassing from the 2014–2015 fissure eruption at the Bárðarbunga volcanic
807 system, Iceland. Journal of Geophysical Research: Solid Earth, 121(3), 1610-1630.

808 Giggenbach, W.F. 1987. Redox processes governing the chemistry of fumarolic gas discharges
809 from White Island, New Zealand. Applied Geochemistry, 2(2), 143-161.

Handley, H.K., Macpherson, C.G., Davidson, J.P., Berlo, K., Lowry, D., 2007. Constraining fluid and sediment contributions to subduction-related magmatism in Indonesia: Ijen Volcanic Complex. Journal of Petrology, 48(6), 1155-1183.

Heap, M.J., Troll, V.R., Kushnir, A.R., Gilg, H.A., Collinson, A.S., Deegan, F.M., Darmawan, H., Seraphine, N., Neuberg, J., Walter, T.R., 2019. Hydrothermal alteration of andesitic lava domes can lead to explosive volcanic behaviour. Nature communications, 10(1), 1-10.

Henley, R.W., Seward, T.M. 2018. Gas–solid reactions in arc volcanoes: Ancient and modern. Reviews in Mineralogy and Geochemistry, 84(1), 309-349.

Ilyinskaya, E., Schmidt, A., Mather, T. A., Pope, F. D., Witham, C., Baxter, P., Jóhannsson, T., Pfeffer, M., Barsotti, S., Singh, A., Sanderson, P., Bergsson, B., McCormick, B., Donovan, A., Peters, N., Oppenheimer, C., Edmonds, M., 2017. Understanding the environmental impacts of large fissure eruptions: Aerosol and gas emissions from the 2014–2015 Holuhraun eruption (Iceland). Earth and Planetary Science Letters, 472, 309-322.

Inguaggiato, C., Iñiguez, E., Peiffer, L., Kretzschmar, T., Brusca, L., Mora-Amador, R., Ramirez, C., Bellomo, S., Gonzalez, G., Rouwet, D., 2018. REE fractionation during the gypsum crystallization in hyperacid sulphate-rich brine: The Poás Volcano crater lake (Costa Rica) exploited as laboratory. Gondwana Research, 59, 87-96.

Inostroza, M., Aguilera, F., Menzies, A., Layana, S., González, C., Ureta, G., Sepulveda, J.P., Scheller, S., Boëhm, S., Barraza, M., Tagle, R., Patzschke, M., 2020. Deposition of metals and metalloids in the fumarolic fields of Guallatiri and Lastarria volcanoes, northern Chile. Journal of Volcanology and Geothermal Research, 393, 106803.

Jessop, D. E., Moune, S., Moretti, R., Gibert, D., Komorowski, J. C., Robert, V., Heap, M., Bosson, A., Bonifacie, M., Deroussi, S., Dessert, C., Rosas-Carbajal, M., Lemarchand, A., Burtin, A., 2021. A multi-decadal view of the heat and mass budget of a volcano in unrest: La Soufrière de Guadeloupe (French West Indies). Bulletin of Volcanology, 83(3), 1-19.

Kagoshima, T., Sano, Y., Takahata, N., Maruoka, T., Fischer, T.P., Hattori, K., 2015. Sulphur geodynamic cycle. Scientific Reports, 5(1), 1-6.

837 Kalacheva, E., Taran, Y., Kotenko, T., Hattori, K., Kotenko, L., Solis-Pichardo, G., 2016.
838 Volcano–hydrothermal system of Ebeko volcano, Paramushir, Kuril Islands: Geochemistry
839 and solute fluxes of magmatic chlorine and sulfur. Journal of Volcanology and Geothermal
840 Research, 310, 118-131.

841 Keith, M., Smith, D. J., Jenkin, G.R., Holwell, D.A., Dye, M.D., 2018. A review of Te and Se
842 systematics in hydrothermal pyrite from precious metal deposits: Insights into ore-forming
843 processes. Ore Geology Reviews, 96, 269-282.

844 Kodosky, L., Keskinen, M., 1990. Fumarole distribution, morphology, and encrustation
845 mineralogy associated with the 1986 eruptive deposits of Mount St. Augustine, Alaska.
846 Bulletin of volcanology, 52(3), 175-185.

847 Komorowski, J.C. 2005. Guadeloupe. Volcanic Atlas of the Lesser Antilles, 65-102.

848 Komorowski, J.C., Legendre, Y., Caron, B., Boudon, G. 2008. Reconstruction and analysis of
849 sub-plinian tephra dispersal during the 1530 AD Soufrière (Guadeloupe) eruption: Implications
850 for scenario definition and hazards assessment. Journal of Volcanology and Geothermal
851 Research, 178(3), 491-515.

852 Le Guern, F. 1988. Ecoulements réactifs à hautes températures, mesures et modélisations
853 (Doctoral dissertation, Paris 7).

854 Le Guern, F., Bernard, A., Chevrier, R.M., 1980. Soufriere of Guadeloupe 1976–1977
855 eruption—Mass and energy transfer and volcanic health hazards. Bulletin volcanologique,
856 43(3), 577-593.

857 Lepel, E.A., Stefansson, K.M., Zoller, W.H., 1978. The enrichment of volatile elements in the
858 atmosphere by volcanic activity: Augustine volcano 1976. Journal of Geophysical Research:
859 Oceans, 83(C12), 6213-6220.

860 Mandon, C.L., Seward, T.M., Christenson, B.W., 2020. Volatile transport of metals and the Cu
861 budget of the active White Island magmatic-hydrothermal system, New Zealand. Journal of
862 Volcanology and Geothermal Research, 398, 106905.

Mandon, C.L., Christenson, B.W., Schipper, C.I., Seward, T.M., Garaebiti, E., 2019. Metal transport in volcanic plumes: a case study at White Island and Yasur volcanoes. Journal of Volcanology and Geothermal Research, 369, 155-171.

Martin, R.S., Mather, T.A., Pyle, D.M., Power, M., Allen, A.G., Aiuppa, A., Horwell, C.J., Ward, E.P.W., 2008. Composition-resolved size distributions of volcanic aerosols in the Mt. Etna plumes. Journal of Geophysical Research: Atmospheres, 113(D17).

Mather, T.A., Pyle, D.M., Oppenheimer, C., 2003. Tropospheric volcanic aerosol. Geophysical Monograph-American Geophysical Union, 139, 189-212.

Metcalfe, A., Moune, S., Komorowski, J. C., Kilgour, G., Jessop, D.E., Moretti, R., Legendre, Y., 2021. Magmatic Processes at La Soufrière de Guadeloupe: Insights from Crystal Studies and Diffusion Timescales for eruption onset. Frontiers in Earth Science, 9, 78.

Moretti, R., Komorowski, J.C., Ucciani, G., Moune, S., Jessop, D., de Chabalier, J.B., Beauducel, F., Bonifacie, M., Burtin, A., Vallée, M., Deroussi, S., Robert, V., Gibert, D., Didier, T., Kitou, T., Feuillet, N., Allard, P., Tamburello, G., Shreve, T., Saurel, J.M., Lemarchand, A., Rosas-Carbajal, M., Agrinier, P., Le Friant, A., Chaussidon, M., 2020a. The 2018 unrest phase at La Soufrière of Guadeloupe (French West Indies) andesitic volcano: Scrutiny of a failed but prodromal phreatic eruption. Journal of Volcanology and Geothermal Research, 393, 106769.

Moretti, R., Moune, S., Robert, V., Jessop, D.E., Didier, T., Bonifacie, M., Komorowski, J.C., 2020b. Intercomparison of geochemical techniques at La Soufrière de Guadeloupe (FWI) volcano: their advantages and their limits over a long-standing unrest. Italian Journal of Geosciences, 139(3), 398-412.

Moune, S., Gauthier, P.J., Delmelle, P., 2010. Trace elements in the particulate phase of the plume of Masaya Volcano, Nicaragua. Journal of Volcanology and Geothermal Research, 193(3-4), 232-244.

Moune, S., Faure, F., Gauthier, P.J., Sims, K.W., 2007. Pele's hairs and tears: natural probe of volcanic plume. Journal of Volcanology and Geothermal Research, 164(4), 244-253.

Moune, S., Moretti, R., Burtin, A., Jessop, D., Didier, T., Robert, V., Bonifacie, M., Tamburello, G., Komorowski, J.C., Allard, P., Buscetti, M. (2022). Gas monitoring of volcanic-hydrothermal plumes in a tropical environment: the case of La Soufriere de Guadeloupe unrest volcano (Lesser Antilles). Frontiers in Earth Sciences, 10: 795760.

Mroz, E.J., Zoller, W.H., 1975. Composition of atmospheric particulate matter from the eruption of Heimaey, Iceland. Science, 461-464.

Nelms, S.M., 2005. Inductively coupled plasma mass spectrometry handbook. CRC press.

Obenholzner, J.H., Schroettner, H., Golob, P., Delgado, H., 2003. Particles from the plume of Popocatépetl volcano, Mexico—the FESEM/EDS approach. Geological Society, London, Special Publications, 213(1), 123-148.

OVSG-IPGP., 2020. Monthly report of the volcanic activity of La Soufriere de Guadeloupe and on the regional seismicity. November 2020.

Peng, X., Jones, B., 2012. Rapid precipitation of silica (opal-A) disguises evidence of biogenicity in high-temperature geothermal deposits: case study from Dagunguo hot spring, China. Sedimentary Geology, 257, 45-62.

Pichavant, M., Poussineau, S., Lesne, P., Solaro, C., Bourdier, J.L., 2018. Experimental parametrization of magma mixing: application to the AD 1530 eruption of La Soufrière, Guadeloupe (Lesser Antilles). Journal of Petrology, 59(2), 257-282.

Pokrovski, G.S., Borisova, A.Y., Bychkov, A.Y. 2013. Speciation and transport of metals and metalloids in geological vapors. Reviews in Mineralogy and Geochemistry, 76(1), 165-218.

Pyle, D.M., Mather, T.A., 2003. The importance of volcanic emissions for the global atmospheric mercury cycle. Atmospheric Environment, 37(36), 5115-5124.

Quisefit, J.P., Toutain, J.P., Bergametti, G., Javoy, M., Cheynet, B., Person, A. 1989. Evolution versus cooling of gaseous volcanic emissions from Momotombo Volcano, Nicaragua: Thermochemical model and observations. Geochimica et Cosmochimica Acta, 53(10), 2591-2608.

916 Reyes, A.G., Trompetter, W.J., Britten, K., Searle, J., 2002. Mineral deposits in the Rotokawa
917 geothermal pipelines, New Zealand. Journal of Volcanology and Geothermal Research, 119(1-
918 4), 215-239.

919 Rosas-Carbajal, M., Komorowski, J.C., Nicollin, F., Gibert, D., 2016. Volcano electrical
920 tomography unveils edifice collapse hazard linked to hydrothermal system structure and
921 dynamics. Scientific reports, 6(1), 1-11.

922 Rose, W.I., Heiken, G., Wohletz, K., Eppler, D., Barr, S., Miller, T., Chuan, R., Symonds, R.
923 B., 1988. Direct rate measurements of eruption plumes at Augustine volcano: A problem of
924 scaling and uncontrolled variables. Journal of Geophysical Research: Solid Earth, 93(B5),
925 4485-4499.

926 Sainlot, N., Vlastelic, I., Moune, S., Rose-Koga, E.F., Schiavi, F., Valade, S., Aguilera, F.,
927 2020. Uptake of gaseous thallium, tellurium, vanadium and molybdenum into anhydrous alum,
928 Lascar volcano fumaroles, Chile. Geochimica et Cosmochimica Acta, 275, 64-82.

929 Sanchez-Yanez, C., Reich, M., Leisen, M., Morata, D., Barra, F., 2017. Geochemistry of metals
930 and metalloids in siliceous sinter deposits: Implications for elemental partitioning into silica
931 phases. Applied Geochemistry, 80, 112-133.

932 Scher, S., Williams-Jones, A.E., Williams-Jones, G., 2013. Fumarolic activity, acid-sulfate
933 alteration, and high sulfidation epithermal precious metal mineralization in the crater of Kawah
934 Ijen Volcano, Java, Indonesia. Economic Geology, 108(5), 1099-1118.

935 Scholtysik, R., Canil, D., 2020. Investigation of the effect of Cl on the transport and
936 sublimation of volatile trace metals in volcanic gases using benchtop fumarole experiments.
937 Journal of Volcanology and Geothermal Research, 395, 106838.

938 Shevko, E.P., Bortnikova, S.B., Abrosimova, N.A., Kamenetsky, V.S., Bortnikova, S.P., Panin,
939 G.L., Zelenski, M., 2018. Trace elements and minerals in fumarolic sulfur: the case of Ebeko
940 Volcano, Kuriles. Geofluids, 2018.

941 Stefánsson, A., Stefánsdóttir, G., Keller, N.S., Barsotti, S., Sigurdsson, Á., Thorláksdóttir, S.
942 B., Pfeffer, M., Eiriksdóttir, E., Jónasdottir, E., von Löwis, S., Gíslason, S.R., 2017. Major
943 impact of volcanic gases on the chemical composition of precipitation in Iceland during the

2014–2015 Holuhraun eruption. Journal of Geophysical Research: Atmospheres, 122(3), 1971-1982.

Symonds, R.B., Gerlach, T.M., Reed, M.H., 2001. Magmatic gas scrubbing: implications for volcano monitoring. Journal of Volcanology and Geothermal Research, 108(1-4), 303-341.

Symonds, R.B., Mizutani, Y., Briggs, P.H., 1996. Long-term geochemical surveillance of fumaroles at Showa-Shinzan dome, Usu volcano, Japan. Journal of Volcanology and Geothermal Research, 73(3-4), 177-211.

Symonds, R.B., Reed, M.H., Rose, W.I., 1992. Origin, speciation, and fluxes of trace-element gases at Augustine volcano, Alaska: Insights into magma degassing and fumarolic processes. Geochimica et Cosmochimica Acta, 56(2), 633-657.

Symonds, R.B., Rose, W.I., Gerlach, T.M., Briggs, P.H., Harmon, R.S., 1990. Evaluation of gases, condensates, and SO 2 emissions from Augustine volcano, Alaska: the degassing of a Cl-rich volcanic system. Bulletin of Volcanology, 52(5), 355-374.

Tamburello, G., Moune, S., Allard, P., Venugopal, S., Robert, V., Rosas-Carbajal, M., Deroussi, S., Kitou, T., Didier, T., Komorowski, J.C., Beauducel, F., de Chabalier, J.B., Le Marchand, A., Le Friant. A., Bonifacie, M., Dessert, C., Moretti, R., 2019. Spatio-temporal relationships between fumarolic activity, hydrothermal fluid circulation and geophysical signals at an arc volcano in degassing unrest: La Soufrière of Guadeloupe (French West Indies). Geosciences, 9(11), 480.

Taran, Y.A., Bernard, A., Gavilanes, J.C., Lunezheva, E., Cortes, A., Armienta, M.A. 2001. Chemistry and mineralogy of high-temperature gas discharges from Colima volcano, Mexico. Implications for magmatic gas–atmosphere interaction. Journal of Volcanology and Geothermal Research, 108(1-4), 245-264.

Taran, Y.A., Hedenquist, J.W., Korzhinsky, M.A., Tkachenko, S.I., Shmulovich, K.I., 1995. Geochemistry of magmatic gases from Kudryavy volcano, Iturup, Kuril Islands. Geochimica et Cosmochimica Acta, 59(9), 1749-1761.

Taran, Y., Zelenski, M., Chaplygin, I., Malik, N., Campion, R., Inguaggiato, S., Pokrovsky, B., Kalacheva, E., Melnikov, D., Kazahaya, R., Fischer, T., 2018. Gas emissions from

volcanoes of the Kuril Island arc (NW Pacific): geochemistry and fluxes. Geochemistry, Geophysics, Geosystems, 19(6), 1859-1880.

Van Hinsberg, V., Berlo, K., Sumarti, S., Van Bergen, M., Williams-Jones, A., 2010. Extreme alteration by hyperacidic brines at Kawah Ijen volcano, East Java, Indonesia: II: Metasomatic imprint and element fluxes. Journal of Volcanology and Geothermal Research, 196(3-4), 169-184.

van Hinsberg, V., Vigouroux, N., Palmer, S., Berlo, K., Mauri, G., Williams-Jones, A., Mckenzie, J., Williams-Jones, G., Fischer, T., 2015. Element flux to the environment of the passively degassing crater lake-hosting Kawah Ijen volcano, Indonesia, and implications for estimates of the global volcanic flux. Geological Society, London, Special Publications, 437(1), 9-34.

Varrica, D., Tamburo, E., Dongarrà, G., Sposito, F., 2014. Trace elements in scalp hair of children chronically exposed to volcanic activity (Mt. Etna, Italy). Science of the Total Environment, 470, 117-126.

Villemant, B., Komorowski, J.C., Dessert, C., Michel, A., Crispi, O., Hammouya, G., Beauducel, F., De Chabalier, J.B., 2014. Evidence for a new shallow magma intrusion at La Soufrière of Guadeloupe (Lesser Antilles): insights from long-term geochemical monitoring of halogen-rich hydrothermal fluids. Journal of Volcanology and Geothermal Research, 285, 247-277.

Yudovskaya, M.A., Tessalina, S., Distler, V.V., Chaplygin, I.V., Chugaev, A.V., Dikov, Y.P., 2008. Behavior of highly-siderophile elements during magma degassing: A case study at the Kudryavy volcano. Chemical Geology, 248(3-4), 318-341.

Zelenski, M.E., Fischer, T.P., De Moor, J.M., Marty, B., Zimmermann, L., Ayalew, D., Nekrasov, A., Karandashev, V.K., 2013. Trace elements in the gas emissions from the Erta Ale volcano, Afar, Ethiopia. Chemical Geology, 357, 95-116.

Zelenski, M., Malik, N., Taran, Y., 2014. Emissions of trace elements during the 2012–2013 effusive eruption of Tolbachik volcano, Kamchatka: enrichment factors, partition coefficients and aerosol contribution. Journal of Volcanology and Geothermal Research, 285, 136-149.